

SPECTROSCOPY OF $Z \sim 6$ *I*-DROPOUT GALAXIES: FREQUENCY OF $LY\alpha$ EMISSION AND THE SIZES OF $LY\alpha$ EMITTING GALAXIES^{1,2,3}

C. C. DOW-HYGELUND⁴, B.P. HOLDEN⁵, R.J. BOUWENS⁵, G.D. ILLINGWORTH⁵, A. VAN DER WEL⁶, M. FRANX⁷, P.G. VAN DOKKUM⁸, H. FORD⁶, P. ROSATI⁹, D. MAGEE⁵, AND A. ZIRM⁶

Draft version July 4, 2018

ABSTRACT

We report on deep spectroscopy using LRIS on Keck I and FORS2 on the VLT of a sample of 22 candidate $z \sim 6$ Lyman Break galaxies (LBGs) selected by the $i_{775} - z_{850} > 1.3$ dropout criterion. Redshifts could be measured for eight objects. These redshifts are all in the range $z = 5.5 - 6.1$, confirming the efficiency of the $i_{775} - z_{850}$ color selection technique. Six of the confirmed galaxies show $Ly\alpha$ emission. Assuming that the 14 objects without redshifts are $z \sim 6$ LBGs, but lack detectable $Ly\alpha$ emission lines, we infer that the fraction of $Ly\alpha$ emitting LBGs with $Ly\alpha$ equivalent widths greater than 20 Å among $z \sim 6$ LBGs is $\approx 30\%$, similar to that found at $z \sim 3$. Every $Ly\alpha$ emitting object in our sample is compact with $r_{hl} \leq 0''.14$. Furthermore, all the $Ly\alpha$ emitting objects in our sample are more compact than average relative to the observed size-magnitude relation of a large *i*-dropout sample (332 candidate $z \sim 6$ objects). We can reject the hypothesis that the $Ly\alpha$ emitting population is a subset of the rest of the $z \sim 6$ LBG population at $>97\%$ confidence. We speculate the small sizes of $Ly\alpha$ emitting LBGs are due to these objects being less massive than other LBGs at $z \sim 6$.

Subject headings: galaxies: evolution — galaxies: formation — galaxies: high-redshift — galaxies: starburst — early universe

1. INTRODUCTION

Distinguishing high redshift galaxies from interlopers at lower redshifts can be a challenging process (Stern & Spinrad 1999). One particularly unique trait of high-redshift galaxies is the continuum break they possess as a result of absorption by neutral hydrogen along the line-of-sight (Madau 1995; Dickinson 1999). Putting together this feature with the particularly blue colors of star-forming galaxies, we have a simple but efficient technique for selecting high-redshift star-forming galaxies (Steidel et al. 1995; Dickinson 1999). This technique has been extensively tested through spectroscopy on numerous Lyman break galaxies (LBGs) at $z \sim 2.5 - 4.5$ (Steidel et al. 1999) and an increasing number

of galaxies and quasars at $z \gtrsim 4$ (Weymann et al. 1998; Spinrad et al. 1998; Dey et al. 1998; Lehnert & Bremer 2003; Nagao et al. 2004; Fan et al. 2001; Bunker et al. 2003; Dickinson et al. 2004; Vanzella et al. 2006). In addition, there are now surveys that exploit narrow-band excess from $Ly\alpha$ emission (see Taniguchi et al. 2003) to compile large (> 20) samples of $Ly\alpha$ emitters (LAEs) at $z \approx 5.7$ (Rhoads et al. 2003; Hu et al. 2004; Shimasaku et al. 2005) and at $z \approx 6.6$ (Kashikawa et al. 2006; Stern et al. 2005).

Several groups, utilizing these techniques, have obtained statistically significant samples of galaxies at $z \sim 6$ (Rhoads & Malhotra 2001; Ajiki et al. 2003; Bouwens et al. 2003, 2004a, 2006; Stanway et al. 2003; Dickinson et al. 2004; Ajiki et al. 2005), as well as identifying candidate galaxies out to $z \sim 7-8$ (Hu et al. 2002; Kodaira et al. 2003; Bouwens et al. 2004b; Taniguchi et al. 2004; Stern et al. 2005; Rhoads et al. 2004; Kneib et al. 2004; Bouwens & Illingworth 2006; Iye et al. 2006). This has led to great progress in our understanding of the early universe, providing us with constraints on both the epoch of reionization (see Loeb & Barkana 2001; Fan et al. 2003; Malhotra & Rhoads 2004) and the evolution of the global star formation rate (SFR) density (Bouwens et al. 2003, 2004a, 2006; Hopkins 2004; Giavalisco et al. 2004). However, to ensure that these results are accurate, it is essential that we understand nature of the galaxy populations being selected by these techniques and can quantify their relation to the underlying population of star-forming galaxies at $z \gtrsim 6$. This is paramount if we are to construct a self-consistent picture of the galaxy population from the different selection techniques. Issues that need to be addressed include (1) quantifying the distribution of $Ly\alpha$ equivalent widths for star-forming galaxies at $z \sim 6$, (2) determining the impact of these

¹ Based on observations taken with the W.M. Keck Observatory, which is operated as a scientific partnership among the California Institute of Technology, the University of California, and NASA.

² Based on observations made with the NASA/ESA *Hubble Space Telescope*, which is operated by the Association of Universities for Research in Astronomy, Inc., under NASA contract NAS 5-26555. These observations are associated with programs 7817, 9270, 9301, 9583, and 9803.

³ Based on observations collected at the European Southern Observatory, Paranal, Chile (LP166.A-0701 and 169.A-045).

⁴ Physics Department, University of California, Santa Cruz, CA 95064; cdow@scipp.ucsc.edu

⁵ Department of Astronomy and Astrophysics, University of California, Santa Cruz, CA 95064; holden@ucolick.org, bouwens@ucolick.org, gdi@ucolick.org, magee@ucolick.org

⁶ Department of Physics and Astronomy, Johns Hopkins University, 3400 North Charles Street Baltimore, MD 21218-2686; wel@pha.jhu.edu, ford@pha.jhu.edu, azirm@pha.jhu.edu

⁷ Leiden Observatory, P.O. Box 9513, J. H. Oort Building, Niels Bohrweg 2, NL-2300 RA, Leiden, Netherlands; franx@strw.leidenuniv.nl

⁸ Department of Astronomy, Yale University, P.O. Box 208101, New Haven, CT 06520-8101; dokkum@astro.yale.edu

⁹ European Southern Observatory, Karl-Schwarzschild-Strasse 2, D-85748 Garching, Germany; prosati@eso.org

results on narrowband and broadband selections, and (3) using search results to construct a self-consistent picture of the galaxy population at $z \gtrsim 6$.

In this study, we utilize spectroscopy to study the nature of $z \sim 6$ i_{775} -dropouts identified by Bouwens et al. (2003, 2004a) in deep ACS imaging data. By contrasting the properties of our spectroscopic sample with similar selections at $z \sim 3$, we examine the evolution of the spectral properties of these sources with redshift. In addition, we pay particular attention to the implications of these results for future studies of high redshift galaxies using either narrowband or broadband selection techniques – noting their respective strengths and complementarity. A brief outline of this paper follows. A summary of the i -dropout sample and spectroscopic observations is presented in §2. In §3 we present the spectra and their interpretations. In §4, we compare our results with those obtained with narrowband selections at $z \sim 6$. In §5, we discuss the fraction of LAEs in the i -dropout sample, as compared with lower redshift samples. We also investigate a possible link between the morphologies of the i -dropouts and their Ly α emission. Finally, in §6 we summarize our findings, and discuss their implications for future high-redshift surveys.

In this paper we adopt the ‘concordance’ cosmology: a Λ -dominated, flat universe with $\Omega_M = 0.3$, $\Omega_\Lambda = 0.7$, and $H_0 = 71 \text{ km s}^{-1} \text{ Mpc}^{-1}$ (Bennett et al. 2003). All magnitudes are given in the AB system (Oke & Gunn 1983). We denote the *Hubble Space Telescope* Advanced Camera for Surveys (ACS) F435W, F606W, F775W, and F850LP passbands as B_{435} , V_{606} , i_{775} and z_{850} respectively.

2. SAMPLE + OBSERVATIONS

2.1. Optical Broadband Dropout-Selected Survey

Our spectroscopic sample was derived from *HST* ACS observations over two separate fields: RDCS 1252.9-2927 (CL1252), a cluster at $z = 1.237$ selected from the ROSAT Deep Cluster Survey (Rosati et al. 1998, 2004), and the Ultra Deep Field parallel fields (UDF PFs; Bouwens et al. 2004a). A $6'$ by $6'$ mosaic of ACS Wide Field Camera i_{775} and z_{850} band images was acquired around CL1252, with $4'$ by $4'$ VLT ISAAC IR imaging of the mosaic center (Lidman et al. 2004). The UDF PFs were imaged with a $4'.5$ by $4'.5$ ACS mosaic in the B_{435} , V_{606} , i_{775} and z_{850} band filters. For further details concerning the imaging data and our photometry over these fields, we refer the reader to Bouwens et al. (2003, 2004a).

The i_{775} and z_{850} band imaging data over these fields allow us to readily select LBGs in the range $5.5 < z < 6.2$ (Bouwens et al. 2003) using an i -dropout criteria. In the case of CL1252, the selection was based upon a $i_{775} - z_{850} > 1.3$ color cut and for the UDF PFs (Bouwens et al. 2004a), a $i_{775} - z_{850} > 1.4$ cut plus a null detection in V_{606} (2σ). Note that the colour selection we use for following up sources in the CL1252 field is more inclusive than the $i_{775} - z_{850} > 1.5$ criterion used in Bouwens et al. (2003). The $i_{775} - z_{850} > 1.3$ criterion used for selection in the CL1252 field resulted from a small systematic error that was present in the early z_{850} ACS zeropoint. The typical error for the $i_{775} - z_{850}$ colors is 0.4 mag. In the case of a non-detection, the i_{775} flux was set to the 2σ upper

limit. The error and upper limits are incorporated into all simulations that determine selection volume for the different samples. A total of 25 i -drops were identified in the CL1252 field, and 40 over the UDF PFs, with 10σ limiting magnitudes of $z_{850} = 27.3$ and 27.8 respectively. This corresponds to surface densities of 0.5 ± 0.1 objects arcmin $^{-2}$ for CL1252, and 1.4 ± 0.2 objects arcmin $^{-2}$ for the UDF PFs.

In Table 1 and Table 2, the objects satisfying the i -dropout criteria for spectroscopic follow-up are listed, along with their z_{850} -band, J -band and K_s -band magnitudes, and $i_{775} - z_{850}$ colors. A total of 22 objects were observed spectroscopically (14 in CL1252 and eight in the UDF PFs). These objects were randomly selected from the entire i -dropout sample for spectroscopic follow-up, except for the most luminous dropout in the CL1252 field (BD38) which was explicitly targeted for follow-up. In addition, i -dropout galaxies were the primary targets for both the CL1252 and UDF PFs spectroscopic observations. The faintest galaxy on our mask had a z_{850} -band magnitude of 27.5.

2.2. Keck I LRIS

We used the Low Resolution Imaging Spectrograph (LRIS) (Oke et al. 1995) on the Keck I 10m telescope for spectroscopic follow-up of all 22 objects in our spectroscopic sample. A total integration time of 16200 s for CL1252 objects and 7200 s for UDF PFs objects was obtained using the 600 line mm $^{-1}$ grating blazed at 8500 Å with a slitlet width of $1''$ and a minimum slitlet length of $10''$. The scale ($\Delta\lambda_{res}$) of this configuration is 1.28 Å per pixel. A series of eight dithered exposures was taken to aid in cosmic ray removal, and to enhance removal of the fringing in the near-IR region of the spectra. The telescope was offset $1''$ - $3''$ along the slits between exposures, which ranged from 1200 to 2250 s in duration. The observations were taken under photometric conditions on the nights of UT 2004 February 13-14.

All data reductions were conducted using a slit mask reduction task developed by Daniel Kelson. This task yields cleaner background subtraction and cosmic ray removal than standard slit spectroscopy procedures (Kelson 2003). By performing the sky subtraction before the data have been rectified, this methodology minimizes reduction errors. One example of this reduction procedure is presented in Figure 1. Wavelength calibration was performed using the night skylines. The spectra were flux calibrated using a sensitivity function derived from observations taken the same night of the spectrophotometric standard HZ44 (Massey et al. 1988; Massey & Gronwall 1990).

2.3. VLT FORS2

Three CL1252 i -drop objects (BD38, BD03, and BD46) were also observed with the Focal Reducer/low dispersion Spectrograph 2 (FORS2) on the 8.2-m VLT YEPUN Unit Telescope in Mask Exchange Unit mode. These objects were observed as part of a large observing program aimed at acquiring very deep spectra of both field and cluster elliptical galaxies in the redshift range 0.6-1.3. We used the 600z grism with the OG590 order separation filter, which yielded a scale element of 1.64 Å per pixel. The data presented here were taken from UT

TABLE 1
PROPERTIES OF OUR RDCS 1252-2927 SPECTROSCOPIC SAMPLE

Object ID	Previous ID ^a	RA	Dec	z_{850}	J	Ks	$i_{775} - z_{850}$	$r_{hl}(\prime\prime)$	z
BD38 ^{b,c}	1252-5224-4599	12 52 56.888	-29 25 55.50	24.3±0.1	24.1±0.1	23.8±0.1	1.5	0.29	5.515
BD03 ^{b,c}	1252-2134-1498	12 52 45.382	-29 28 27.11	25.6±0.1	25.2±0.4	>25.6	>2.1	0.18	5.980
BD27	...	12 52 51.902	-29 26 28.60	25.6±0.1	26.1±0.4	25.8±0.4	1.5	0.11	...
BD58	1252-2585-3351	12 52 52.283	-29 28 04.74	25.7±0.1	25.6±0.3	25.4±0.3	2.0	0.20	...
BD44	1252-5058-5920	12 53 01.745	-29 26 03.87	25.9±0.2	26.3±0.4	25.5±0.4	>1.8	0.19	...
BD46 ^{b,d}	...	12 53 05.424	-29 24 26.22	26.1±0.1	NA	NA	1.6	0.14	5.914
BD57	...	12 52 49.441	-29 27 53.24	26.1±0.2	25.7±0.3	24.9±0.2	1.5	0.19	...
BD00 ^d	...	12 52 42.927	-29 29 20.05	26.1±0.1	NA	NA	1.3	0.11	5.942
BD66	...	12 52 54.624	-29 24 56.18	26.1±0.1	NA	NA	1.4	0.13	...
BD40	...	12 52 59.511	-29 26 58.43	26.3±0.1	26.2±0.3	25.9±0.4	1.3	0.15	...
BD22	...	12 52 53.346	-29 27 10.58	26.5±0.2	NA	NA	1.4	0.13	...
BD62	1252-3729-4565	12 52 56.746	-29 27 07.63	26.7±0.2	26.3±0.3	>26.2	>1.8	0.12	...
BD48	1252-3497-809	12 52 42.754	-29 27 18.89	27.0±0.2	NA	NA	>1.6	0.11	...
BD36	...	12 52 54.944	-29 25 57.52	27.1±0.1	26.3±0.4	25.2±0.4	1.5	0.11	...

NOTE. — Right ascension (hours, minutes, seconds) and declination (degrees, arcminutes, arcseconds) use the J2000 equinox. All magnitudes given are AB. An entry of NA indicates that the object was outside the ISAAC coverage we had on CL1252 (Lidman et al. 2004). Each of these objects were observed for four hours with LRIS.

^a Bouwens et al. (2003).

^b FORS2 22.3 hr integrated spectra also obtained.

^c Lacking detectable Ly α emission; absorption line redshift.

^d Ly α emission detected; emission line redshift.

TABLE 2
PROPERTIES OF OUR UDF PARALLEL SPECTROSCOPIC SAMPLE

Object ID	Previous ID ^a	RA	Dec	z_{850}	$i_{775} - z_{850}$	$r_{hl}(\prime\prime)$	z
UDF PFs1 i0	...	03 32 35.604	-27 57 37.51	25.5±0.1	1.9	0.25	...
UDF PFs1 i1	...	03 32 34.892	-27 57 10.74	25.7±0.1	1.5	0.11	...
GOODS i6 0 ^b	...	03 32 39.803	-27 52 57.88	26.1±0.1	1.4	0.10	5.540
UDF PFs i4 ^b	UDFP1-3851-2438	03 32 43.959	-27 56 43.87	26.3±0.1	1.6	0.11	5.857
UDF PFs i9	UDFP1-4650-3354	03 32 40.707	-27 57 24.28	26.4±0.1	1.7	0.16	...
UDF PFs i1 ^b	UDFP1-2954-1152	03 32 48.368	-27 55 54.82	26.9±0.2	1.5	0.09	6.005
UDF PFs i2 ^b	UDFP1-2309-1628	03 32 46.410	-27 55 24.32	27.1±0.1	>2.5	0.10	6.083
UDF PFs i0 ^c	UDFP1-3407-1028	03 32 48.952	-27 56 16.97	27.5±0.2	1.7	0.10	...

^a Bouwens et al. (2004a).

^b Ly α emission detected.

^c This object's LRIS spectrum was contaminated by bleeding from an alignment star spectrum. Therefore it is excluded from the sample.

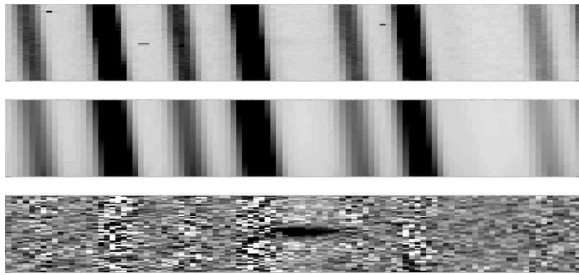


FIG. 1.— An illustration of the reduction process for our two dimensional spectral data. The upper panel shows the unredduced spectrum, the middle panel shows a two dimensional fit to the background, and the lower panel is the reduced spectrum.

2003 February 28 through March 2 and April 27 through May 24 with a median seeing of $0''.65$ and clear conditions. The observations were carried out in a series of four dithered exposures with equal exposure times ranging from 14 to 30 minutes each, yielding a total integration time of 22.3 hours for the sources. All exposures are added and weighted such that optimal signal-to-noise ratios were obtained. Details concerning the data reduction are provided in van der Wel et al. (2005).

3. RESULTS

3.1. Keck Data

Six emission line objects were detected out of the observed 22 object sample. No other spectral features were found (including continuum) in the remaining spectra. Figures 2a - f show our spectra of these objects, with lines evident at 8440 Å, 8404 Å, 8514 Å, 8609 Å, 8335 Å, and 7950 Å. Since O II $\lambda 3727$ would be resolved into a doublet structure with our spectral resolution, this interpretation for these lines could clearly be rejected. Moreover, line interpretations as H β $\lambda 4861.3$, H α $\lambda 6562.8$, and O III $\lambda 5006.8$, 4958.9 could also be discarded due to the lack of nearby lines and the $i_{775} - z_{850} > 1.3$ colors (strong continuum breaks) of our objects. For objects BD00, BD46, UDF PFs i1, and UDF PFs i2, the asymmetry of the line profiles, with absorption on the blue side, is consistent with absorption by a thick Ly α forest. Therefore, it seems quite clear that these emission lines are Ly α $\lambda 1215.67$, placing these objects at $z = 5.942$, 5.9214, 6.005, and 6.083, respectively. For UDF PFs i4 and GOODS i6 0, the emission features are heavily contaminated by sky lines, making it difficult to ascertain their level of asymmetry and thus whether they are likely

$\text{Ly}\alpha$. We tentatively identify these emission features as $\text{Ly}\alpha$ placing these objects at $z = 5.857$ and 5.540 , respectively. However, in the discussion which follows, we shall also consider the implications that these objects are null-detections or low-redshift contaminants.

To quantify the asymmetry of the four uncontaminated emission lines, we adopted the two asymmetry parameters developed by Rhoads et al. 2003. The “wavelength ratio”, a_λ , and “flux ratio”, a_f are defined as,

$$a_w = \frac{\lambda_{10,r} - \lambda_p}{\lambda_p - \lambda_{10,b}} \quad (1)$$

$$a_f = \frac{\int_{\lambda_p}^{\lambda_{10,r}} f_\lambda d\lambda}{\int_{\lambda_{10,b}}^{\lambda_p} f_\lambda d\lambda} \quad (2)$$

respectively. Here, λ_p is the wavelength of the peak of the emission, and $\lambda_{10,b}$ and $\lambda_{10,r}$ are the wavelengths where the flux exceeds 10% of its peak value on the blue and red side of the emission. The resulting values, shown in Table 3, range from $a_w=1.8$ - 2.6 and $a_f=1.4$ - 2.4 . This is in agreement with values determined from $\text{Ly}\alpha$ emitting objects at $z \approx 4.5$ (Dawson et al. 2004), and at $z \sim 5.7$ (Rhoads et al. 2003). These asymmetry parameters are inconsistent with those of the $z \approx 1$ O II $\lambda 3727$ doublet ($a_w \leq 1$ and $a_f \leq 1$; Dawson et al. (2004)). Note that for object BD46, the FORS2 spectrum (see §3.2.1) was used to calculate asymmetry parameters.

The spectrum of UDF PFs i0 was contaminated by bleeding from an alignment star, impeding detection of $\text{Ly}\alpha$ emission or a continuum. Thus, this object is excluded from our sample in the analysis below.

The two objects UDF PFs i1 ($z_{850} = 26.9$) and UDF PFs i2 ($z_{850} = 27.1$) are among the faintest $z > 5$ objects in the z_{850} band to be selected by the Lyman break technique with confirmed redshifts, very similar to the objects GLARE 3001 and 3011, with $z_{850} = 26.37 \pm 0.06$ and 27.15 ± 0.12 respectively (Stanway et al. 2004b). Furthermore, UDF PFs i2 is faintest object in our sample (excluding UDF PFs i0), and is the object with the highest confirmed redshift.

Table 3 gives the measured redshifts, $\text{Ly}\alpha$ fluxes ($f_{\text{Ly}\alpha}$), rest-frame equivalent widths ($W_{\text{Ly}\alpha}$), and FWHMs of the six $\text{Ly}\alpha$ emitting LBGs. We measured the flux in the emission lines between the red dotted lines illustrated in Figures 2 and 3. In some cases, there were residuals from the sky subtraction that could contaminate the line flux. We estimated this additional contribution from the sky lines by measuring the residual flux in two-dimensional sky-subtracted spectrum outside of the extraction region used for the one-dimensional spectrum. All values quoted were measured directly from the spectra, and do not account for flux lost due to HI gas absorption in the objects. Therefore, the quoted fluxes are lower limits. The observed emission fluxes from our $\text{Ly}\alpha$ emitting sample are very similar to those found for other $z \sim 6$ objects selected by the i -dropout method (Bunker et al. 2003; Stanway et al. 2004a,b), and for $z \approx 5.7$ and $z \approx 6.6$ $\text{Ly}\alpha$ emitters selected using narrowband filters (Hu et al. 2004; Rhoads et al. 2003; Lehnert & Bremer 2003; Ajiki et al. 2003; Kurk et al. 2004; Taniguchi et al. 2004; Stern et al. 2005; Nagao et al. 2004; Rhoads et al. 2004). To determine the continuum for each spectrum,

we assumed it satisfied a power law of the form

$$f(\lambda) = f_o(\lambda/0.9\mu\text{m})^\beta \quad (3)$$

with $\beta = -1.1$, which is the average of 198 $\text{Ly}\alpha$ emitting LBGs at $z \sim 3$ (Shapley et al. 2003). f_o was determined by fitting the z_{850} magnitude. The equivalent widths of the $\text{Ly}\alpha$ emissions were calculated directly from these estimated continua. These widths were not very sensitive to the assumed value of β .

3.2. VLT Data

3.2.1. BD46

The two-dimensional FORS2 spectrum of BD46 showed a robust emission line at the central wavelength of 8406 \AA . Two- and one-dimensional extracted spectra for this emission are shown in Figure 3a. A clear asymmetric profile for the line is seen, which we identify as $\text{Ly}\alpha$ yielding a redshift of $z=5.914$ for this source. Furthermore, a weak continuum was detected redward of the emission, with $f = 3.4 \pm 1.0 \text{ counts \AA}^{-1}$, shown in Fig. 3b. One item to note is BD46’s $\text{Ly}\alpha$ emission was detected with LRIS before the VLT data was available. Our methodology accurately measured this redshift (it was within $\Delta z = 0.0005$ of the FORS value), despite a much weaker signal due to the smaller integration time in our Keck LRIS data.

3.2.2. BD03

While this object was undetected in the LRIS (4 hour integration) spectrum, the FORS2 spectrum shown in Figure 4 contains a noisy but clearly flat continuum redward of 8500 \AA , with a sharp discontinuity at $8485 \pm 3 \text{ \AA}$, where the flux drops to approximately zero blueward of 8400 \AA . Using a constant step function to fit the continuum, we find the average flux density above the discontinuity is $f^{\text{red}}(8500 - 9100 \text{ \AA}) = 5 \pm 1 \text{ counts \AA}^{-1}$. Below the break, this reduces to $f^{\text{blue}}(7700 - 8300 \text{ \AA}) = 1 \pm 1 \text{ counts \AA}^{-1}$, consistent with no detected flux.

This discontinuity is much larger than would be expected from UV/optical spectral breaks of galaxies at rest wavelengths 4000 \AA [D(4000)], 2900 \AA [B(2900)], and 2640 \AA [B(2640)] (Stern et al. 2000; Spinrad et al. 1997, 1998). Another option is that this object is a radio-loud broad absorption line quasar. Such objects can have large continuum breaks of this amplitude. However, such objects also possess very red near-IR colors (Hall et al. 1997), unlike BD03 ($J - K_s < -0.03$). Furthermore, the resolved morphology of BD03 is atypical for luminous AGNs at high redshift, which are generally unresolved.

The abruptness of the break and the lack of slope in the continuum at larger wavelengths are strong signs that the discontinuity is due to absorption by intergalactic HI gas. Coupling this with the $i_{775} - z_{850} > 2.1$ colors (the second reddest in our spectroscopic sample), we interpret this object as being a starburst galaxy at $z = 5.98 \pm 0.1$. Using the LRIS spectrum we place an upper flux limit of $8.0 \times 10^{-19} \text{ ergs cm}^{-2} \text{ s}^{-1}$ on the $\text{Ly}\alpha$ emission.¹⁰

¹⁰ All flux limits are for a 3σ detection extracted over 4 \AA ($\approx 3\Delta\lambda_{\text{res}}$). Note that Stanway et al. (2004a) quoted a 10.5 hr DEIMOS spectra flux limit of $2.0 \times 10^{-18} \text{ ergs cm}^{-2} \text{ s}^{-1}$, which is for a 5σ detection extracted over 8 \AA .

TABLE 3
OBJECTS WITH DETECTABLE $\text{Ly}\alpha$ EMISSION

Object ID	z	$f_{\text{Ly}\alpha}^{\text{a,c}}$ (10^{-17} ergs cm^{-2} s^{-1})	$W_{\text{Ly}\alpha}^{\text{b,c}}$ (\AA)	FWHM ^c (\AA)	a_w/a_f^{d}
BD46	5.914	0.90	24	6	1.9/1.8
BD00	5.942	3.50	150	10	1.8/1.4
GOODS i6 0	5.540	1.34	31	19	...
UDF PFs i4	5.857	0.70	34	10	...
UDF PFs i1	6.005	1.10	65	13	2.6/2.4
UDF PFs i2	6.083	0.96	64	10	2.3/1.5

^a Flux from $\text{Ly}\alpha$ emission.

^b Measured rest-frame equivalent width.

^c Not corrected for IGM absorption.

^d Emission line asymmetry parameters (Rhoads et al. 2003)

3.2.3. *BD38*

This object was also undetected in the LRIS observations, but yields a strong continuum in the FORS2 spectrum. Figure 5 shows the two- and one-dimensional spectra of the object, along with the ACS and ISAAC imaging. A precipitous continuum break is clearly seen at $\approx 7900 \text{ \AA}$, reducing the continuum from 27 ± 1 to 0 ± 1 counts \AA^{-1} . Also, several strong absorption features are found at 8205.77 \AA , 8485.38 \AA , 8498.43 \AA , 8699.72 \AA , 9079.21 \AA , and 9140.84 \AA in the spectrum. Associating the break with the UV optically thick $\text{Ly}\alpha$ forest, and the absorption lines with the strong interstellar absorption features typical of LBGs at lower redshifts (see Shapley et al. 2003; Ando et al. 2004), yields a redshift determination of 5.515 ± 0.003 .

BD38 is an unusually bright i -dropout. Its z_{850} -band magnitude is 24.3, making this object more than 1.3 mag brighter than any other i -dropout in our spectroscopic or photometric sample. In fact, to our knowledge, this object is still the brightest $z \sim 6$ LBG discovered to date with a confirmed redshift. The complete spectrum, along with a more thorough analysis of this object is presented in Dow-Hygelund et al. (2005).

4. DISCUSSION

4.1. Confirmation and Contamination

Of the total 21 galaxies in our spectroscopic sample (excluding UDF PFs i0), we identified spectral features for eight objects. Of these eight, we confirmed that six i -dropouts from our sample are $z \sim 6$ galaxies, with the strong possibility that two more are. Therefore, the success rate of our survey is assuredly 29%, and most likely 38%. For the smaller integration times obtained with LRIS (4 hours), the completeness drops to 25% (19% disregarding GOODS i6 0 and UDF PFs i4). The confirmation rate in our longer 22.3 hr FORS2 integrations is 100% (three out of three). Interestingly, the two reddest $i_{775} - z_{850}$ color objects, the two brightest z_{850} objects, and the faintest z_{850} object in our sample are confirmed $z \sim 6$ galaxies.

There was no evidence from the spectra that any of the objects in our sample are low-redshift contaminants despite the long integration times. This is consistent with these objects being $z \sim 6$ continuum objects without strong $\text{Ly}\alpha$ emission. However, if we associate the emission lines of GOODS i6 0 and UDF PFs i4 with those of low redshift interlopers (for which we have no evidence) the contamination of the sample could be as

high as 14%, though this is unlikely. Support for this point is provided by the low resolution spectroscopy conducted by Malhotra et al. (2005) using the ACS grism to test the i -dropout selection. Using a liberal color cut of $i_{775} - z_{850} > 0.9$ (versus our $i_{775} - z_{850} > 1.3$ criterion), they verified that 23 out of 29 candidate i -dropouts showed a strong continuum break indicative of galaxies at $z \sim 6$. In addition, they found that a colour cut of $i_{775} - z_{850} > 1.3$, while suffering from modest (20-30%) incompleteness, is subject to a contamination rate of only 7% (one out of 14).¹¹ Since the estimated contamination in the large (506 object) i -dropout selection of Bouwens et al. (2006) is similarly small ($\leq 8\%$), the present findings are perhaps not too surprising. This lends strong support to the notion that the objects in our sample without detectable features are primarily unconfirmed $z \sim 6$ galaxies, and are not low redshift interlopers.

To see if any of the unconfirmed galaxies in our CL1252 spectroscopic sample are low- z cluster members, we coadded the LRIS spectra associated with these sources, in an effort to increase the signal to noise of the observations. If these objects were predominately $z = 1.23$ early-type contaminants, a break at $\approx 8800 \text{ \AA}$ would appear. No continuum break was detected in the coadded spectra, nor was any excess continuum found. Therefore, we concluded that the majority of the objects in our sample are not cluster members. We should note however that this null detection is not very surprising considering that BD38 and BD03, which are the brightest objects in our sample and are confirmed $z \sim 6$ objects via the FORS2 observations, were undetected in the LRIS observations. The main conclusion of this analysis is that deeper spectroscopy is necessary to ascertain the nature of these galaxies.

4.2. Star Formation Rate

Aside from $\text{Ly}\alpha \lambda 1215.67$, no other emission lines were found in our sample of galaxies with $\text{Ly}\alpha$ emission. Another sometimes strong line in our wavelength range is the rest-UV line N v $\lambda 1240$. This emission feature is strong in active galactic nuclei (AGNs),

¹¹ This contaminant was a star. The methodology of Bouwens et al. (2003, 2004a, 2006) uses the SExtractor stellarity parameter (Bertin & Arnouts 1996) to exclude stars from our i -dropout selection. Hence, this contaminant would likely have been rejected from our spectroscopic sample. Thus, our null contamination results are consistent with the findings of Malhotra et al. (2005).

with line ratios from a composite quasar spectra of $\langle f_{\text{Ly}\alpha}/f_{\text{NV}} = 4.0 \rangle$ (Osterbrock 1989). The flux limits at rest-frame 1240 Å are $f_{\text{NV}} < (0.8, 0.8, 1.0, 2.4, 2.2, 1.0) \times 10^{-18}$ ergs cm $^{-2}$ s $^{-1}$, implying lower limits of the $f_{\text{Ly}\alpha}/f_{\text{NV}} > (11.3, 44.8, 13.4, 2.9, 5.0, 9.6)$ line ratios. Furthermore, no object in our sample was detected in Chandra or XMM-Newton X-ray imaging data (Rosati et al. 2004; Giacconi et al. 2002). The lack of any N v $\lambda 1240$ emission or X-ray detection suggests that the Ly α emission is not produced by an AGN. Thus, we believe the Ly α photons are primarily from hot young stellar populations consistent with the Ly α emitting objects being starbursting galaxies.

Now we estimate the star formation rates of our eight confirmed and 13 unconfirmed objects in our $z \sim 6$ sample. Two different methods are used, the first relying the Ly α emission flux ($SFR_{\text{Ly}\alpha}$) to make this estimate, and the second relying on the UV-continuum flux (SFR_{UV}). The relationship between the Ly α flux and the SFR of a galaxy is given by

$$SFR_{\text{Ly}\alpha} = 9.1 \times 10^{-43} L_{\text{Ly}\alpha} M_{\odot} \text{ yr}^{-1} \quad (4)$$

where $L_{\text{Ly}\alpha}$ is the Ly α luminosity in units of ergs s $^{-1}$, assuming the Salpeter initial mass function with $(m_{\text{lower}}, m_{\text{upper}}) = (0.1 M_{\odot}, 100 M_{\odot})$ (Salpeter 1955; Brocklehurst 1971; Kennicutt 1998). The SFRs determined by this method yield lower limits, due to absorption of Ly α photons by dust grains within the galaxy and by the Ly α forest (Hu et al. 2002). The SFRs can also be derived from the UV continuum luminosities (L_{UV}) at $\lambda = 1500$ Å, and using the following relation

$$SFR_{\text{UV}} = 1.4 \times 10^{-28} L_{\text{UV}} M_{\odot} \text{ yr}^{-1} \quad (5)$$

where L_{UV} is in units of ergs s $^{-1}$ Hz $^{-1}$ (Madau et al. 1998). For the nine objects with ISAAC imaging, the slope of the continuum was derived from the z_{850} , J , and K_s magnitudes assuming the UV spectrum can be described by $f_{\lambda} \propto \lambda^{\beta}$. The continuum slope used for the remaining objects was the consistent value of $\beta = -2.0$ found from *HST*/NICMOS imaging of 26 i -dropout objects in the UDF (Stanway et al. 2005; Bouwens et al. 2006). We adopted a different β than that used in §3.1, because of the observed β dependence on Ly α emission strength at $z \sim 3$ (Shapley et al. 2003). For the objects in our sample for which we cannot measure redshifts, the mean redshift for i -dropouts in our selection, $z = 5.9$ (Bouwens et al. 2003), is assumed.

For objects in the CL1252 field, we used the results of Lombardi et al. (2005) to correct for gravitational amplification by the cluster potential. For each object, we assumed a Non-Singular Isothermal Sphere lensing model with a free central position. This yields a best-fitting velocity dispersion of 1185 km s $^{-1}$. Again, for the non-detected objects the mean redshift $z = 5.9$ was used. The resulting gravitational magnifications are presented in the second column of Table 4. Most objects are two or more Einstein radii away, being only weakly lensed. However BD22 and BD62 are close to the Einstein radius, and therefore the magnifications quoted for these sources are highly uncertain. Hereafter only delensed values for objects in the CL1252 field are quoted, except for BD22 and BD62 where observed values are retained.

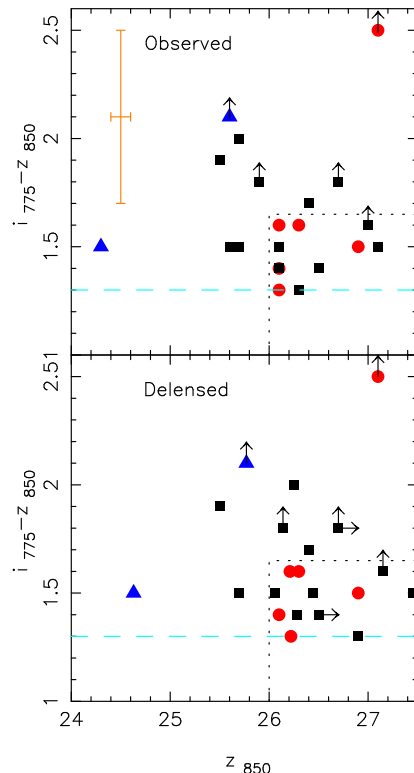


FIG. 6.— Observed (upper) and delensed (lower) $i_{775}-z_{850}$ colors versus z_{850} -band magnitudes for our spectroscopic sample. The black squares are sources where no spectral features were found red circles are the sources with Ly α emission, and blue triangles are sources with no detectable Ly α emission but for which we can derive a redshift (BD03 and BD38). Objects undetected in the i_{775} band are shown at their 2σ lower limits and include upward arrows. The sources in CL1252 that are not delensed are shown with right arrows. The upper left orange error bars are typical for objects detected in the i_{775} filter. Our $i_{775}-z_{850} > 1.3$ selection criterion is denoted with the blue dashed line. Aside from UDF PFs i2, the distribution of Ly α emitters is constrained to $z_{850} \geq 26.1$ and $i_{775}-z_{850} \leq 1.6$ (demarcated by dotted lines). In the observed plot almost half (9 out of 21) lie outside this region. However, this trend is absent after delensing the objects. Ly α emitting objects likely have bluer $i_{775}-z_{850}$ colors than other i -dropouts as a result of the contribution of Ly α flux to the i_{775} -band magnitudes (see Figure 7).

In Table 4 we present $L_{\text{Ly}\alpha}$, L_{UV} , $SFR_{\text{Ly}\alpha}$, and SFR_{UV} for the Ly α emitting objects in our sample. Errors in L_{UV} and SFR_{UV} are derived from the z_{850} -band flux errors. As is seen elsewhere (Hu et al. 2002; Kodaira et al. 2003; Ajiki et al. 2003), for the five Ly α emitting objects the ratio $SFR_{\text{Ly}\alpha}/SFR_{\text{UV}}$ ranges widely from 27% to 127%. This is most likely due to absorption of Ly α photons by the IGM (Hu et al. 2002).

4.3. Selection Completeness for Ly α Emitters

Ly α $\lambda 1215.67$ emission is by far the most prominent spectral feature we can use for redshift determination of $z > 5$ objects. When the Ly α emission is strong, it can have an effect on the observed broadband fluxes. At $z < 6$, Ly α flux falls in the i -band, yielding $i-z$ colors that are smaller than without such emission. This effect is notable in Figure 6, where we show the $i_{775}-z_{850}$ colors vs. z_{850} -band magnitudes of our sample. Aside from UDF PFs i2, which is at $z = 6.083$, the Ly α emitting objects inhabit the region $i_{775}-z_{850} \leq 1.6$.

TABLE 4
STAR FORMATION RATES FOR OUR $z \sim 6$ SAMPLE

Object ID	μ^a	$L_{Ly\alpha}^b$ ($10^{42} h_{0.7}^{-2}$ ergs s $^{-1}$)	L_{UV}^c ($10^{28} h_{0.7}^{-2}$ ergs s $^{-1}$ Hz $^{-1}$)	$SFR_{Ly\alpha}^d$ ($h_{0.7}^{-2} M_{\odot}$ yr $^{-1}$)	SFR_{UV}^e ($h_{0.7}^{-2} M_{\odot}$ yr $^{-1}$)
BD38	1.3	<0.5 ^f	27.1±2.7	<0.5	38.1±3.8
BD03	1.2	<0.3 ^f	10.0±1.0	<0.4	13.4±1.3
BD00	1.1	13.24	6.8±0.7	12.1	9.5±1.0
BD46	1.1	3.37	6.7±0.7	3.1	9.5±1.0
GOODS i6 0	...	4.31	6.7±0.7	3.9	9.4±1.0
UDF PFs i4	...	2.56	6.1±0.6	2.3	8.5±1.0
UDF PFs i1	...	4.27	3.5±0.7	3.9	5.1±1.0
UDF PFs i2	...	3.84	3.1±0.3	3.5	4.3±0.4
UDF PFs i0	...	NS	12.9±1.3	...	18.0±1.8
UDF PFs-IDROP1	...	NS	12.9±1.3	...	18.0±1.8
BD27	1.5	NS	7.6±0.8	...	10.6±1.1
BD44	1.2	NS	7.3±1.5	...	10.1±2.0
BD58	1.6	NS	6.6±0.7	...	9.3±1.0
BD66	1.2	NS	6.2±0.6	...	8.67±0.9
UDF PFs1 i9	...	NS	5.6±0.6	...	7.9±0.8
BD57	1.3	NS	5.3±1.1	...	7.7±1.5
BD22	4.22	NS	5.1±1.0 ^g	...	7.2±1.4 ^g
BD62	35.1	NS	4.1±0.8 ^g	...	6.2±1.2 ^g
BD40	1.6	NS	3.9±0.4	...	5.4±0.5
BD48	1.2	NS	2.7±0.5	...	3.8±0.8
BD36	1.4	NS	2.4±0.2	...	3.4±0.3

NOTE. — Uncertainties in L_{UV} and SFR_{UV} are derived from the z_{850} -band flux errors. All quoted luminosities and star formation rates for CL1252 cluster objects are corrected for possible lensing, except for BD22 and BD62 where the observed values are used. An entry of NS indicates that no spectral features were detected for the object. Where no redshift could be determined, the quoted UV luminosities are for the object at the mean redshift $z = 5.9$ estimated for i -dropout selections (Bouwens et al. 2003).

^a Gravitational magnification due to the CL1252 cluster potential

^b Ly α luminosity.

^c UV continuum luminosity at $\lambda=1500$ Å.

^d SFR derived from $L_{Ly\alpha}$.

^e SFR derived from L_{UV} .

^f No detectable Ly α emission.

^g Not corrected for gravitational lensing and thus highly uncertain.

Moreover, from Vanzella et al. (2006); Vanzella et al. (2005); Dickinson et al. (2004); Nagao et al. (2004); Stanway et al. (2004a,b); Bunker et al. (2003) and this work, only two confirmed Ly α emitting objects have been detected by the i -dropout technique for $z < 5.78$. Once Ly α redshifts into the z_{850} band, the decrement can be larger than it would be without emission, such as for the $z = 6.33$ Ly α emitting i -dropout object SDF J132440.6+273607 discovered by Nagao et al. (2004).

In Figure 7, we present the redshift distribution of spectroscopically confirmed $z \sim 6$ i -dropouts. The upper histogram contains objects from this work and Stanway et al. (2004a,b); Malhotra et al. (2005); Vanzella et al. (2006). The lower histogram only contains those objects which have measurable Ly α emission. In addition, the expected distribution of i -dropouts from the simulations of Bouwens et al. (2003, 2006) are plotted. From these curves it is evident that as the strength of Ly α emission increases, the mean redshift of the i -dropout population increases quite noticeably, while the width of this distribution narrows somewhat. Hence, there is a substantial bias against lower redshift ($z \lesssim 5.7$), strong ($W_{Ly\alpha} \geq 50$ Å) Ly α emitting i -dropouts being selected as i -dropouts. However, this effect is small for weaker ($W_{Ly\alpha} = 25$ Å) Ly α emitting objects. Considering that over half of the Ly α emitting objects in our sample have $W_{Ly\alpha} \leq 30$ Å, this should only result in a modest bias. In § 5.1 we discuss this issue further.

To understand how Ly α emission affects i -dropout selection and how this influence evolves with redshift, we

modeled the spectra of the Hu et al. (2004) (hereafter Hu04) sample of 19 confirmed $z \approx 5.7$ LAEs, all identified by a narrowband selection. We plot the colors for Hu04 in Figure 8. Spectra of these objects were assumed to satisfy the power law given in Eq. 3. The flux decrement due to the IGM was modeled as a simple transmission coefficient, where initial values for the fit were obtained from the tables of Songaila (2004). The continuum level was set to zero blueward of the Lyman limit λ_{912} . The IGM transmission, f_o , and total Ly α emission integrated flux were varied as three fit parameters until the quoted NB_{8150} , Cousins Z , and Cousins I magnitudes in Hu04 were reproduced using the IRAF software package Synphot. These fiducial spectra were then artificially redshifted or blueshifted across the space probed by the i_{775} -dropout technique in intervals of $\Delta z = 0.1$. At each interval, the i_{775} and z_{850} magnitudes were recomputed using the model for each galaxy.

By directly applying our search criterion on these calculated i_{775} and z_{850} magnitudes, we can determine the efficiency of the i_{775} -drop method at selecting LAEs at various redshifts. Using the relation

$$n = \int_{z_1=5.5}^{z_2=6.2} \rho(z) dV(z) \approx \sum_{i=1}^7 \rho(z_i) \Delta V(z_i) \\ = \sum_{i=1}^7 \bar{\rho} * \epsilon(z_i) \Delta V(z_i) \quad (6)$$

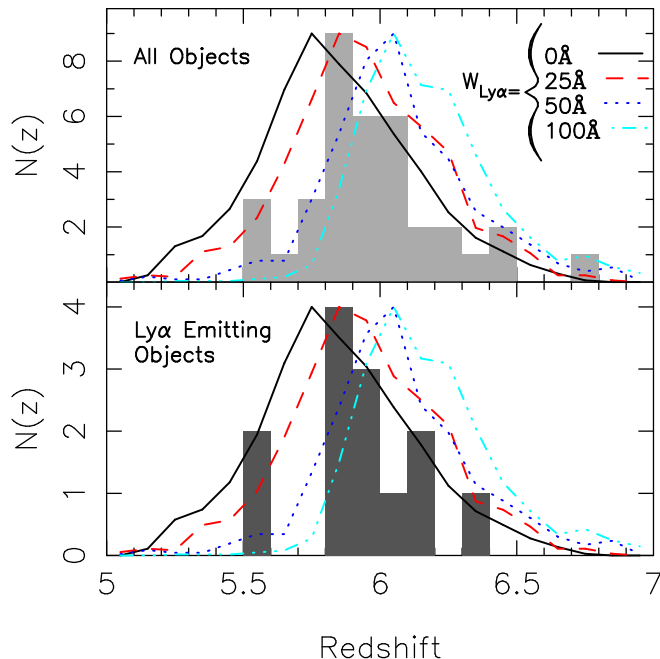


FIG. 7.— Observed distribution of spectroscopically confirmed $z \sim 6$ i -dropouts ($i_{775} - z_{850} > 1.3$). The upper histogram contains confirmed sources from this work and Stanway et al. (2004a), Stanway et al. (2004b), Malhotra et al. (2005), and Vanzella et al. (2006). The lower histogram contains objects with detectable Ly α emission. Overplotted are simulated redshift distributions for four different Ly α equivalent widths $W_{\text{Ly}\alpha}$, indicating the impact of these equivalent widths on the redshift distribution of the i -dropout selection. Overall, the simulations respectably encompass the observed distribution, and suggest that most star-forming galaxies at $z \sim 6$ only have modest Ly α equivalent widths.

where n is the expected value of LAEs, $\rho(z)$ is the volume density of Hu04 LAEs at redshift z , $\bar{\rho}$ is the true volume density of Hu04's objects, $\epsilon(z_i)$ is the fraction of Hu04 LAEs we would select at redshift z_i (i.e., selection probability), $\Delta V(z_i)$ is the volume element for the redshift interval $z_{i+1} - z_i$, and the sum ranges from $z_1 = 5.5$ to $z_7 = 6.1$. This relation yields an expectation value of 3.0 strong LAEs in the CL1252 field.

This expectation value is an upper limit due to two additional effects. First, the probability of a $z \sim 6$ object being selected by the $i_{775} - z_{850}$ dropout technique is a strong function of redshift, dropping off rapidly at the highest redshifts probed (Bouwens et al. 2003, 2006). This is due to surface brightness selection effects at work at the high-redshift end of our $z \sim 6$ i -dropout selection (see Bouwens et al. 2006). Second, Ly α emission redshifted into the OH bands will be much more difficult to detect than emission in the region between the bands, and so the comoving volume probed will be smaller than we assumed. Mitigating this fact is the quoted flux limit of Hu04 is 2×10^{-17} ergs cm^{-2} s^{-1} . This is slightly greater than the average flux limit for our CL1252 spectra for a Ly α emission in the redshift interval probed (1.9×10^{-17} ergs cm^{-2} s^{-1}).

Hence, we believe the expectation value of 3.0 LAEs to be consistent with our spectroscopic results of two Ly α emitting LBGs (BD00 and BD46) in our CL1252 sample of 12 objects. Moreover, it appears our survey

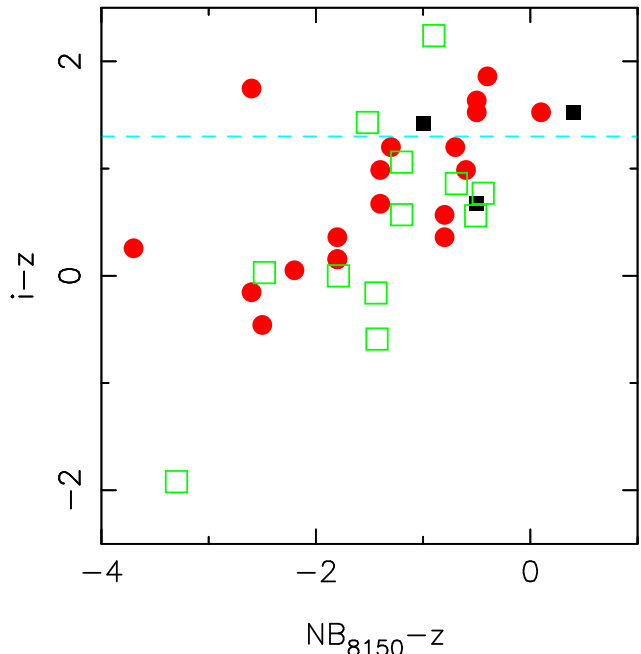


FIG. 8.— $i-z$ vs. NB_{8150-z} color distribution of two narrowband selected samples. The red circles are spectroscopically confirmed $z \approx 5.7$ Ly α emitters and the black filled squares are unconfirmed objects from Hu et al. (2004). The green open squares are narrowband excess candidate Ly α emitters from Ajiki et al. (2005). No excess flux in the z_{850} -band was measured for two objects in this sample; hence they are excluded from the plot. A typical i -dropout color selection of $i_{775} - z_{850} > 1.3$ is shown by the blue dashed line. Nine out of 33 objects would fall within our i -dropout selection. Hence, the i -band dropout technique seems to select $\approx 30\%$ of the $z \approx 5.7$ Ly α emitters found by narrowband surveys. It is relevant to note that four of these are the weakest emitters of the confirmed sample of Hu et al. (2004). The other objects do not meet our selection criterion because of the contribution of Ly α flux to the i -band magnitude (see Figure 7). As noted in Fig. 7, this selection bias is not a problem for higher redshift ($z \geq 6$) LAEs.

is complete in identifying objects that have measurable Ly α emission. Coupling this with our likely minimal low-redshift contamination rates (see §4.1) suggests that Ly α emitting LBGs only represent a fraction of i -dropout selected $z \sim 6$ LBGs.

We estimated the total number of expected LAEs over the redshift range of our i -dropout selection assuming the Hu04 volume density and the Bouwens et al. (2003) covolume. This yields a strict upper limit of 5.6 expected LAEs in our CL1252 sample. From this estimate, the i -dropout selection misses at most 2.6/5.6, or $\approx 46\%$ of the total LAE population, though most of those missed are at the low redshift end of the i -dropout range.

5. TRENDS IN $Z \sim 6$ LYMAN BREAK GALAXIES

5.1. Fraction of Ly α Emitting Galaxies

In our sample, we find six objects (four if GOODS i6 0 and UDF PFs i4 are disregarded) with rest-frame equivalent widths strong enough to be detected as narrowband excess objects ($W_{\text{Ly}\alpha} \geq 20$ Å). Thus 29% (19%) of our sample (excluding UDF PFs i0) would be recovered by narrowband surveys. Similar results of 33%, 33% and 31% are found by Stanway et al. (2004a), Stanway et al. (2004b), and Vanzella et al. (2006). These observations, and the results of the Ly α emission completeness test of §4.3, suggest that Ly α emitting objects represent $\approx 30\%$

of i -dropout spectroscopic samples.

However, just because the fraction of i -dropouts with Ly α emission is 30% does not imply that the same thing is true for the $z \sim 6$ population as a whole. In §4.3, and easily seen in Fig. 7, the $i_{775} - z_{850} > 1.3$ color cut biases our selection against the inclusion of lower redshift ($z < 5.8$) objects with strong Ly α emission ($\geq 50\text{\AA}$). This suggests that the effective selection volumes (and redshift distributions) of i -dropouts with significant Ly α emission may be quite different from the distribution without such emission.

This can be accounted for by utilizing the simulations of Bouwens et al. (2006) (see Fig. 7) to determine the effective search volumes, and corresponding densities, for objects of different Ly α equivalent widths. For the distribution of $W_{Ly\alpha}$ in our sample (i.e., three objects with $W_{Ly\alpha}=25\text{\AA}$, two with $W_{Ly\alpha}=50\text{\AA}$, and one with $W_{Ly\alpha}=100\text{\AA}$) these simulations imply that $32 \pm 10\%$ of star-forming galaxies at $z \sim 6$ have $W_{Ly\alpha} \geq 20\text{\AA}$, and $7 \pm 6\%$ have $W_{Ly\alpha} \geq 100\text{\AA}$.¹² In the situation where every Ly α emitting object in our sample has $W_{Ly\alpha}=100\text{\AA}$ and spectroscopy misses every object with $z \geq 6.15$, this fraction increases to $46 \pm 11\%$. This case is an upper limit given our assumptions. A lower limit of $25 \pm 10\%$ is determined, if the emission line objects GOODS i6 0 and UDF PFs i4 are lower redshift contaminants. A similar Ly α emitting fraction of $32 \pm 14\%$ (upper limit of $47 \pm 16\%$) is found using the results of Stanway et al. (2004a).

These results are similar to those obtained from Shapley et al. (2003), who analyzed spectra of over 1000 $z \sim 3$ LBGs. Though Shapley et al. (2003) selected their LBGs photometrically using a two-color cut, the extra color is used to remove potential low-redshift contaminants. As noted in § 4.1, the expected contamination of our survey is small; hence, we believe our $z \sim 6$ LBG survey is similar enough to warrant comparison. Shapley et al. (2003) find that only 25% of their sample of $z \sim 3$ LBGs have $W_{Ly\alpha} \geq 20\text{\AA}$, and $\sim 2\%$ have $W_{Ly\alpha} \geq 100\text{\AA}$. This is similar to the value we determine from our observed Ly α fraction (as well as that of Stanway et al. (2004a)). Moreover, the fraction of $z \sim 3$ objects with $W_{Ly\alpha} \geq 20\text{\AA}$ is within 2σ of our $z \sim 6$ upper limit. Therefore, it appears that there is no strong evolution in the fraction of Ly α emitting objects between $z \sim 3$ to $z \sim 6$.

Differing results are found by Shimasaku et al. (2006), who compare the $z \sim 6$ LBG luminosity function of Bouwens et al. (2006) with that derived from their $z \approx 5.7$ LAE sample. These authors determine that nearly every $z \sim 6$ LBG with $M_{UV} \lesssim -20$ ($z_{850} \lesssim 26.6$ mag) should have $W_{Ly\alpha} \geq 20\text{\AA}$. In fact, Shimasaku et al. (2006) argue that the fraction of $z \sim 6$ LBGs with $W_{Ly\alpha} \geq 100\text{\AA}$ is $\approx 80\%$. Clearly these results are inconsistent with our analysis above. At best, the Shimasaku et al. (2006) fraction is a factor of ≈ 2 too high. To be consistent with our survey, the spectroscopic efficiency we calculated in § 4.3 must be a factor of > 10 too low, a situation we consider highly unlikely given our agreement

with the results of Hu et al. (2004) and Stanway et al. (2004a). Hence, we believe that the Ly α emitting fraction of nearly unity found by Shimasaku et al. (2006) must be wrong. This may be at least partially due to the mild evolution in the luminosity function which will occur between $z \approx 5.9$ (the mean redshift of the Bouwens et al. (2006) i -dropout selection) to $z \approx 5.7$, which is not accounted for by Shimasaku et al. (2006).

5.2. Luminosities and Star Formation Rates

Objects in our sample with measurable Ly α emission all have observed z_{850} -band magnitudes of 26.1 or fainter, populating the faintest 70% of the upper panel of Figure 6. Furthermore, the brightest two objects in our CL1252 sample were confirmed $z \sim 6$ LBGs without any detectable Ly α emission. However, after deblending the sources in our CL1252 sample (lower plot of Fig. 6), this luminosity segregation of Ly α emitting objects is removed. The Ly α emitting LBGs found by Stanway et al. (2004a) have z_{850} -band magnitudes of 25.48 ± 0.03 , 26.37 ± 0.06 , and 27.15 ± 0.12 . Aside from the brightest object in the Stanway et al. (2004a) sample and the extremely bright ($z_{850} = 24.7$) object of Bunker et al. (2003), all confirmed $z \sim 6$ Ly α emitting i -dropout objects have z_{850} -band magnitudes in excess of 26.

The average star formation rate derived from the UV continuum (SFR_{UV}) of our entire sample (excluding the $6L^*$ object BD38) is $8.8 \pm 3.9 h_{0.7}^{-2} M_{\odot} \text{ yr}^{-1}$. This value increases slightly to $9.2 \pm 4.4 M_{\odot} \text{ yr}^{-1}$ if we exclude Ly α emitting objects. The average SFR_{UV} of Ly α emitting objects is $7.7 \pm 2.2 M_{\odot} \text{ yr}^{-1}$. Hence, the SFR_{UV} of Ly α emitting objects appears to be similar to that of the i -dropout population in general. Shapley et al. (2003) find at $z \sim 3$ that Ly α emitting galaxies with stronger Ly α emission have lower star formation rates. However, as noted by these authors, this trend could be at least partially due to selection effects. Given the relatively small size of our sample, and the large uncertainties (up to a factor of 10) inherent in UV continuum derived SFRs (see Papovich et al. 2005), our results do not allow us to make strong statements about the SFRs of Ly α emitting LBGs relative to the population as a whole.

5.3. Correlation between Ly α Emission and Galaxy Size

In Figure 10 we show z_{850} -band images ($1''.5$ thumbnails) for our entire spectroscopic sample (excluding UDF PFs i0). The uppermost six thumbnails are the confirmed Ly α emitting LBGs, the two thumbnails in the bottom row are the confirmed $z \sim 6$ objects with no detectable Ly α emission, and the middle 13 are objects with no clear spectral features. The Ly α emitting LBGs all have compact morphologies and show no morphological disturbances. However, the morphologies of BD38 and BD03 are very disturbed and extended, with “plumes” extending from a “core”. Furthermore, the undetected objects overall have much more extended morphologies than the objects with detected Ly α emission.

Similarly, Stanway et al. (2004a,b) confirmed Ly α emitting i -dropout objects have compact morphologies in the z_{850} band, with $0''.09 \leq r_{hl} \leq 0''.14$. Moreover, SBM03#01 also appears compact in *HST* NICMOS 1.1 μm F110W-band and 1.6 μm F160W-band imaging (Eyles et al. 2005). Interestingly, the Ly α -emitting

¹² We compute the errors on the fraction of LAEs assuming a binomial distribution. This assumes systematic errors are small.

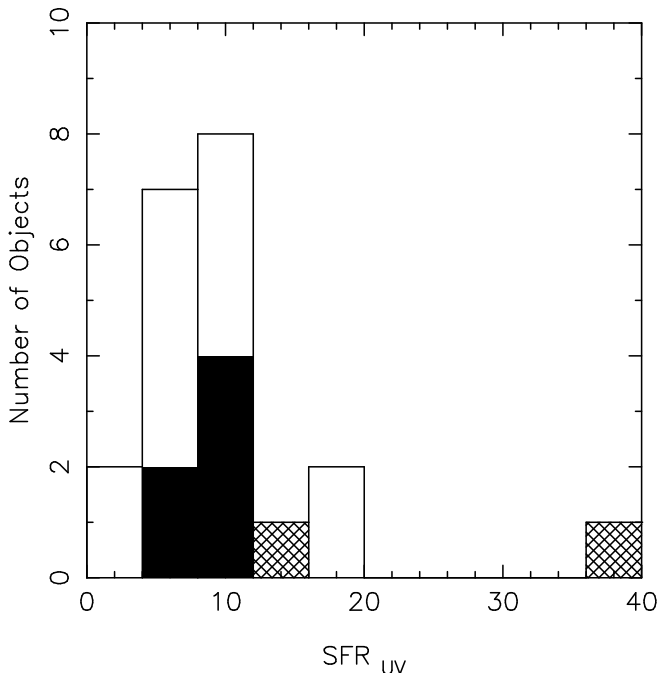


FIG. 9.— Histograms of SFR_{UV} for our spectroscopic sample. Sources in the CL1252 field were corrected for lensing by the cluster potential, except for objects BD22 and BD62 where the correction was highly uncertain. The solid filled histogram are Ly α emitting objects, and the cross hatched are the confirmed $z \sim 6$ continuum objects lacking detectable Ly α emission. The Ly α emitting objects appear to have SFR_{UV} very similar to the sample average (excluding the $6L_*$ galaxy BD38).

$z = 5.78$ galaxy SBM03#03 discovered by Bunker et al. (2003) also has a very compact morphology ($r_{hl} \leq 0''.08$; marginally resolved in ACS imaging), despite being exceedingly bright ($z_{850} = 24.7$) for an i -dropout. This is in contrast to BD38, a similarly bright ($z_{850} = 24.6$) i -dropout in our spectroscopic sample, but which is much more extended ($r_{hl} = 0''.25$) and lacking Ly α emission.

In the upper panel of Figure 11 we plot the r_{hl} versus z_{850} -band magnitude for sources in our spectroscopic sample. The red circles are Ly α emitting LBGs, the blue triangles represent BD38 and BD03 (sources with a continuum break), and the black squares are i -dropouts in our sample without any clear spectral features. The CL1252 objects have been delensed. Shown with purple dots are the 332 i -dropouts identified by Bouwens et al. (2006) over the two GOODS fields. Also included (red stars) are the four previously confirmed Ly α emitting LBGs of Bunker et al. (2003) and Stanway et al. (2004a,b) noted above, where the half-light radii and z_{850} -band magnitudes quoted are taken from Bouwens et al. (2006)¹³. The purple line in Fig. 11 denotes a linear fit to the i -dropout sample (purple dots) of Bouwens et al. (2006). Objects with half-light radii smaller than the FWHM of the z_{850} -band PSF ($0''.09$; blue dash-dot line in figure), fainter than our magnitude limit ($z_{850} > 27.8$), or brighter than $z_{850} = 25.0$ (due to a scarcity of bright sources) were not included in the fit. No sources from our spectroscopic sample were included in the fit.

¹³ Object GOODS-N i Drop 6 of Stanway et al. (2004a) is not included, due to its uncertain line identification

We want to test the hypothesis that sources with Ly α emission are smaller on average than the i -dropout population in general. We chose not to use a χ^2 test, because it assumes a Gaussian scatter around the best-fit distribution. A better test is the Rank-Sum test utilizing only the half-light radii of our spectroscopic sample. Using this test to compare our spectroscopic sample with the Bouwens et al. (2006) i -dropout sample, we find that the half-light radii of the galaxies in our spectroscopic sample are significantly (at $\geq 94\%$ confidence) smaller than those of Bouwens et al. (2006). Restricting the Rank-Sum test to include only objects in our spectroscopic sample also supports the hypothesis that Ly α emitting i -dropouts are smaller than the rest of our sample at $\geq 97\%$ confidence. Hence, Ly α emitting i -dropouts seem to be morphologically distinct from other i -dropouts.

One potential exception to this rule is the object UDF 5225 of Rhoads et al. (2005), which has a “plume” of $1''$ extending from a compact “core”. This object was selected as a V_{606} -dropout, has a spectroscopic redshift of $z = 5.480$, and is too blue ($i_{775} - z_{850} \approx 0.5$) to be selected by i -dropout methods. However, even if we assumed that this object passed our color selection, the surface brightness of the plume is below our limiting surface brightness, due to shallower photometry than the UDF. Our deepest photometry (UDF PFs) of the object would only contain the brighter compact “core”. Hence, this object would not appear abnormal for Ly α emitting objects in our sample.

Note that the nature of the vast majority of the objects (332 in total) used in our larger i -dropout sample is not known; however from the discussion above, approximately 30% of these objects should be Ly α emitting LBGs. If so, this would mitigate the differences observed between the sizes of Ly α emitting LBGs and those from the i -dropout population in general (which include a significant fraction of Ly α emitting sources). Hence, the size-luminosity discrepancy between Ly α emitting and non-emitting LBGs would be larger than quoted here.

This morphological difference may be due to the influence of the Ly α emission on the z_{850} -band flux. To date, the only confirmed $z \sim 6$ Ly α emitting i -dropout with NICMOS imaging is SBM03#01 (Eyles et al. 2005), which, as noted above, is compact in both $1.1 \mu\text{m}$ F110W-band and $1.6 \mu\text{m}$ F160W-band imaging. Hence, the compact morphology of this LBG cannot simply be the result of its Ly α emission alone. NICMOS imaging of many more i -dropouts with confirmed Ly α emission is needed to determine the overall relevance of Ly α emission to the z_{850} -band morphology of these objects.

One potential physical explanation of this size deviation could lie in the masses of these objects. Ly α emitting objects at $z \sim 3-4$ are found to have smaller stellar masses than objects lacking this emission (Overzier et al. 2006; Gawiser et al. 2006). This suggests that these objects may be associated with less massive dark matter haloes. One would make a similar inference for the masses of these objects using the observation that these objects are less dusty on average (Shapley et al. 2003; Gawiser et al. 2006), thereby having fainter dust-corrected luminosities, than sources with no observable Ly α emission. Assuming this translates to $z \sim 6$, and using the well-known correlation between size and mass (Mo et al. 1998), we would expect Ly α emitting objects to appear smaller on

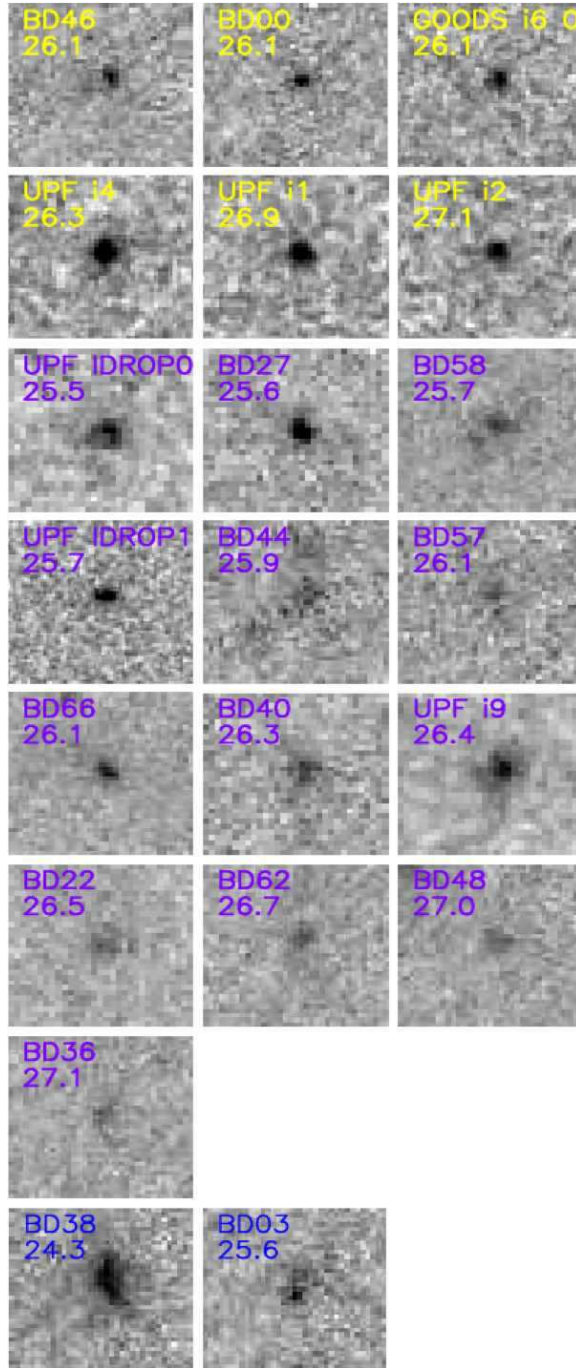


FIG. 10.— Thumbnail images of the entire spectroscopic sample in the z_{850} -band ($1''.5$ on a side). UDF PFs is abbreviated as UPF. The upper six thumbnails are our $\text{Ly}\alpha$ emitting sample, the lowest two are the confirmed $z \sim 6$ objects that are undetected in $\text{Ly}\alpha$ (BD38 and BD03), and the middle 13 are objects without any observed spectral features. The morphologies of BD38 and BD03 are much more disturbed than the $\text{Ly}\alpha$ emitting LBGs. Furthermore, the majority of the undetected, fainter objects have a similar distorted morphology, in contrast to the very compact appearance of the $\text{Ly}\alpha$ emitting LBGs.

average, which is what we observe.

We note that the recent results of Lai et al. (2006) on a sample of 12 $z \sim 5.7$ LAEs over the HDF-North GOODS area could be seen to support this finding. Lai et al. (2006) found that 3 of the 12 sources were clearly detected in the IRAC data and inferred masses of $10^9 M_{\odot}$ to $10^{10} M_{\odot}$ through detailed stellar population modelling. While these masses are comparable to similar luminosity i -dropouts studied over the GOODS fields

(Yan et al. 2006; Eyles et al. 2006), the vast majority of LAEs in the Lai et al. (2006) sample (9 out of 12) are not detected in the GOODS IRAC imaging and hence will be significantly less massive than the 3 IRAC-detected LAEs. Though clearly a more careful comparison between these populations is needed, this suggests that $z \sim 5.7$ LAEs, on average, are somewhat less massive than the typical $z \sim 6$ star-forming galaxy.

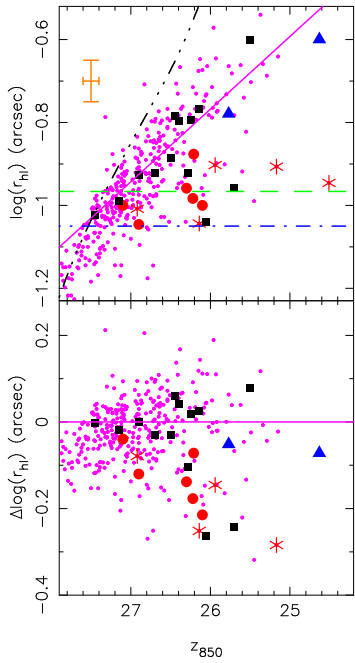


FIG. 11.— (Upper panel) Half-light radius versus z_{850} -band magnitude. The small purple dots represent a sample of 332 i -dropouts selected over the GOODS fields (Bouwens et al. 2006). The red stars are previously spectroscopically-confirmed $z \sim 6$ Ly α emitting LBGs (Bunker et al. 2003; Stanway et al. 2004a,b; Vanzella et al. 2006). The other symbols are the same as Figure 6. The black dot-dash-dot line is the surface brightness selection limit of the Bouwens et al. (2006) sample. The purple line denotes the best linear fit to this sample (purple dots; other objects excluded). The vertical orange error bar of $\sigma = 0.05$ dex is the scatter in the fit. The horizontal error bar is the typical photometric uncertainty. The blue dash-dot line is the FWHM of the z_{850} -band PSF and represents a reasonable floor below which our size measurements become quite uncertain. (Lower panel) Residuals from the linear fit. The Bunker et al. (2003) object is outside the plot window ($\Delta \log r_{hl} = -0.49$). All Ly α emitting objects have half-light radii smaller than is typical for the 332 i -dropouts of Bouwens et al. (2006). A Rank-Sum test performed on the objects from our spectroscopic sample supports the hypothesis (at $\geq 97\%$ confidence) that Ly α emitting i -dropouts (6 objects from our sample) are smaller than the objects without such emission (14 objects from our spectroscopic sample). Furthermore, the Ly α emitting objects have a fairly constant size ($r_{hl} = 0.11 \pm 0.01$) over the entire range of luminosities probed.

5.4. Preselecting Galaxies with Ly α Emission

One interesting aspect of this morphology dependence on Ly α emission strength is in its potential to preselect Ly α emitting i -dropouts for spectroscopic follow-up, similar to what is achieved in narrowband surveys. Confirmation rates of i -dropout selected $z \sim 6$ LBGs are rather low ($\approx 30\%$) due to the low S/N of these objects in the continuum and the small fraction of LBGs with Ly α emission (§5.1). From our spectroscopic sample, we note that a simple size cut $\Delta \log(r_{hl}) \leq -0.05$ and magnitude cut $z_{850} \geq 25.9$ would select five (83%) of the Ly α emitting LBGs, while rejecting all but two (15%) of the sources without detectable Ly α emission. This would increase our success rate for spectroscopic confirmation by more than a factor of three.

6. CONCLUSIONS

We have obtained spectroscopic observations of 22 i -dropouts drawn from two deep ACS fields. These

dropouts were selected to have $i_{775} - z_{850}$ colors greater than 1.3. Spectroscopic redshifts for eight $z \sim 6$ objects in the RDCS 1252-2927 and Ultra Deep Field Parallel fields were derived. We thereby confirm the effectiveness of the i -dropout technique of Bouwens et al. (2003, 2004a) in isolating a statistically relevant sample of $5.5 \leq z \leq 6.2$ star-forming galaxies.

No clear case of contamination by low-redshift sources was found in this sample. Together with the results of the complementary ACS Grism survey of Malhotra et al. (2005), this suggests our spectroscopic sample is dominated ($\geq 90\%$) by galaxies at $z \sim 6$. Six of the confirmed $z \sim 6$ objects possess measurable Ly α emission, with z_{850} -band magnitudes ranging from 26.1 to 27.1. The two brightest objects in our CL1252 sample are continuum sources, lacking detectable Ly α emission, but show clear evidence for a Lyman break.

We compare our findings with other $z \sim 6$ i -dropout surveys, $z \approx 5.7$ narrowband surveys, and with the global properties of LBGs at $z \sim 3$ to determine the nature and composition of $z \sim 6$ galaxies. Our findings are as follows:

1. Significant ($W_{Ly\alpha} \gtrsim 20\text{\AA}$) Ly α emission is detected in the spectra of only 30% of i -dropout objects. Utilizing the model redshift distributions of Bouwens et al. (2006) to control for selection biases, we infer that only $32 \pm 10\%$ of star-forming galaxies at $z \sim 6$ show significant ($W_{Ly\alpha} \gtrsim 20\text{\AA}$) Ly α emission (§5.1: Figure 7), with an upper bound of $46 \pm 11\%$. Moreover, the $W_{Ly\alpha}$ of these objects on average are much smaller than those found for narrowband-selected LAEs. Since these trends are also evident in the LBG population at $z \sim 3$ (Shapley et al. 2003), this suggests that there is no strong change in the fraction of Ly α emitting objects in LBG population from $z > 5$ to $z < 4$.
2. The i -dropout technique misses $\approx 70\%$ of narrowband selected $z \approx 5.7$ LAEs. Moreover, the LAEs i -dropout surveys do select show the weakest Ly α emission. This is a consequence of the Ly α emission in the i_{775} -band flux at $z \leq 5.9$. However, the selection efficiency increases strongly with redshift, due to Ly α emission shifting from the i_{775} to z_{850} bands. By $z \sim 6$, every z_{850} -band detected Ly α emitter would be sampled by i -dropout techniques. Using the simulations in §5.1, we expect to miss 10-46% of the LAE population with our i -dropout selection.
3. Ly α emitting LBGs have similar z_{850} -band magnitudes and UV SFRs to those without detectable emission. However, no Ly α emitting object in our sample has $z_{850} < 26.1$.
4. The size of Ly α emitting objects is more compact than predicted from the observed size-luminosity relation of 332 i -dropout galaxies. One possible explanation for this trend is that sources with Ly α emission may be systematically less massive than the typical i -dropout.

Most importantly, these results suggest that Ly α emitting objects only constitute a modest fraction of the

LBGs at $z \sim 6$ and thus do not provide us with a representative sample.

These results have important implications for how surveys for star-forming galaxies at $z \sim 6$ should be conducted. First, it appears that our spectroscopic success rates can be significantly enhanced by targeting *i*-dropouts with compact z_{850} -band morphologies. From our sample, we find the criteria $z_{850} \geq 25.9$ and $\Delta \log r_{hl} \leq -0.05$ selects $\geq 80\%$ of Ly α emitting objects, while rejecting $\geq 80\%$ of the remaining sample.

Second, it appears wide-area narrowband surveys miss $\approx 70\%$ of the broadband-selected LBG population at $z \sim 6$, and as seen in Figure 11 the objects they do find are intrinsically different from the *i*-dropout LBG population as a whole. On the other hand, broadband surveys miss the strongest Ly α emitters at $5.5 \leq z \leq 5.8$ that narrowband surveys sample. Therefore, it appears a combi-

nation of surveys – taking advantage of the strengths of both narrowband and broadband selection techniques – will be necessary to obtain a complete characterization of the star-forming population at $z \sim 6$.

We would like to thank Dan Kelson for useful discussions concerning spectral reduction, and David Koo for his helpful insights. ACS was developed under NASA contract NAS5-32864, and this research was supported by NASA grant NAG5-7697. The authors wish to recognize and acknowledge the very significant cultural role and reverence that the summit of Mauna Kea has always had within the indigenous Hawaiian community. We are most fortunate to have the opportunity to conduct observations from this mountain.

REFERENCES

- Ajiki, M., Mobasher, B., Taniguchi, Y., Shioya, Y., Nagao, T., Murayama, T., & Sasaki, S. S. 2005, in press (astro-ph/0510672)
- Ajiki, M., et al. 2003, AJ, 126, 2091
- Ando, M., Ohta, K., Iwata, I., Watanabe, C., Tamura, N., Akiyama, M., & Aoki, K. 2004, ApJ, 610, 635
- Bennett, C. L., et al. 2003, ApJS, 148, 97
- Bertin, E. & Arnouts, S. 1996, A&AS, 117, 393
- Bouwens, R. J., Illingworth, G. D., Blakeslee, J. P., & Franx, M. 2006, in press (astro-ph/0509641)
- Bouwens, R. J., & Illingworth, G. D. 2006, Nature, 443, 189
- Bouwens, R. J., et al. 2003, ApJ, 595, 589
- Bouwens, R. J., et al. 2004a, ApJ, 606, L25
- Bouwens, R. J., et al. 2004b, ApJ, 616, L79
- Brocklehurst, M. 1971, MNRAS, 153, 471
- Bunker, A. J., Stanway, E. R., Ellis, R. S., McMahon, R. G., & McCarthy, P. J. 2003, MNRAS, 342, L47
- Dawson, S., et al. 2004, ApJ, 617, 707
- Dey, A., Spinrad, H., Stern, D., Graham, J. R., & Chaffee, F. H. 1998, ApJ, 498, L93+
- Dickinson, M. 1999, in AIP Conf. Proc. 470: After the Dark Ages: When Galaxies were Young (the Universe at $2 \leq z \leq 5$), 122–+
- Dickinson, M., et al. 2004, ApJ, 600, L99
- Dow-Hygelund, C. C., et al. 2005, ApJ, 630, L137
- Eyles, L. P., Bunker, A. J., Stanway, E. R., Lacy, M., Ellis, R. S., & Doherty, M. 2005, MNRAS, 364, 443
- Eyles, L., Bunker, A., Ellis, R., Lacy, M., Stanway, E., Stark, D., & Chiu, K. 2006, MNRAS, in press, astro-ph/0607306
- Faber, S. M., et al. 2003, in Instrument Design and Performance for Optical/Infrared Ground-based Telescopes. Proceedings of the SPIE, Volume 4841, pp. 1657-1669
- Fan, X., et al. AJ, 122, 2833
- Fan, X., et al. 2003, AJ, 125, 1649
- Gawiser, E., et al. 2006, ApJ, 642, L13
- Giacconi, R., et al. 2002, VizieR Online Data Catalog, 213, 90369
- Giavalisco, M., et al. 2004, ApJ, 600, L103
- Hall, P. B., Martini, P., Depoy, D. L., & Gatley, I. 1997, ApJ, 484, L17+
- Hopkins, A. M. 2004, ApJ, 615, 209
- Hu, E. M., Cowie, L. L., Capak, P., McMahon, R. G., Hayashino, T., & Komiyama, Y. 2004, AJ, 127, 563
- Hu, E. M., Cowie, L. L., McMahon, R. G., Capak, P., Iwamuro, F., Kneib, J.-P., Maihara, T., & Motohara, K. 2002, ApJ, 568, L75
- Iye, M., et al. 2006, Nature, 443, 186
- Kashikawa, N., et al. 2006, ApJ, 648, 7
- Kelson, D. D. 2003, PASP, 115, 688
- Kennicutt, R. C. 1998, ARA&A, 36, 189
- Kneib, J., Ellis, R. S., Santos, M. R., & Richard, J. 2004, ApJ, 607, 697
- Kodaira, K., et al. 2003, PASJ, 55, L17
- Kurk, J. D., Cimatti, A., di Serego Alighieri, S., Vernet, J., Daddi, E., Ferrara, A., & Ciardi, B. 2004, A&A, 422, L13
- Lai, K., Huang, J.-S., Fazio, G., Cowie, L. L., Hu, E. M., & Kakazu, Y. 2006, ApJ, in press, astro-ph/0610572
- Lehnert, M. D. & Bremer, M. 2003, ApJ, 593, 630
- Lidman, C., Rosati, P., Demarco, R., Nonino, M., Mainieri, V., Stanford, S. A., & Toft, S. 2004, A&A, 416, 829
- Loeb, A. & Barkana, R. 2001, ARA&A, 39, 19
- Lombardi, M., et al. 2005, ApJ, 623, 42
- Madau, P. 1995, ApJ, 441, 18
- Madau, P., Pozzetti, L., & Dickinson, M. 1998, ApJ, 498, 106
- Malhotra, S., et al. 2005, ApJ, 626, 666
- Malhotra, S. & Rhoads, J. E. 2002, ApJ, 565, L71
- , 2004, ApJ, 617, L5
- Malhotra, S., Wang, J. X., Rhoads, J. E., Heckman, T. M., & Norman, C. A. 2003, ApJ, 585, L25
- Massey, P. & Gronwall, C. 1990, ApJ, 358, 344
- Massey, P., Strobel, K., Barnes, J. V., & Anderson, E. 1988, ApJ, 328, 315
- Mo, H. J., Mao, S., & White, S. D. M. 1998, MNRAS, 295, 319
- Mo, H. J. & White, S. D. M. 1996, MNRAS, 282, 347
- Nagao, T., et al. 2004, ApJ, 613, L9
- Oke, J. B., et al. 1995, PASP, 107, 375
- Oke, J. B. & Gunn, J. E. 1983, ApJ, 266, 713
- Osterbrock, D. E. 1989, Astrophysics of gaseous nebulae and active galactic nuclei (Mill Valley, CA, University Science Books)
- Overzier, R., et al. 2006, ApJ, submitted
- Papovich, C., GOODS, f. t., & MIPS GTO teams. 2005, in press (astro-ph/0601408)
- Phillips, A. C., Faber, S., Kibrick, R., Wallace, V., & DEIMOS Team. 2002, Bulletin of the American Astronomical Society, 34, 1320
- Rhoads, J. E., et al. 2003, AJ, 125, 1006
- Rhoads, J. E. & Malhotra, S. 2001, ApJ, 563, L5
- Rhoads, J. E., et al. 2005, ApJ, 621, 582
- Rhoads, J. E., Xu, C., Dawson, S., Dey, A., Malhotra, S., Wang, J., Jannuzi, B. T., Spinrad, H., & Stern, D. 2004, ApJ, 611, 59
- Rosati, P., della Ceca, R., Norman, C., & Giacconi, R. 1998, ApJ, 492, L21+
- Rosati, P., et al. 2004, AJ, 127, 230
- Salpeter, E. E. 1955, ApJ, 121, 161
- Shapley, A. E., Steidel, C. C., Pettini, M., & Adelberger, K. L. 2003, ApJ, 588, 65
- Shimasaku, K., Ouchi, M., Furusawa, H., Yoshida, M., Kashikawa, N., & Okamura, S. 2005, PASJ, 57, 447
- Shimasaku, K., et al. 2006, PASJ, 58, 313
- Songaila, A. 2004, AJ, 127, 2598
- Spinrad, H., Dey, A., Stern, D., Dunlop, J., Peacock, J., Jimenez, R., & Windhorst, R. 1997, ApJ, 484, 581
- Spinrad, H., Stern, D., Bunker, A., Dey, A., Lanzetta, K., Yahil, A., Pascarelle, S., & Fernández-Soto, A. 1998, AJ, 116, 2617
- Stanway, E., McMahon, R., & Bunker, A. 2005, MNRAS, 359, 1184

- Stanway, E. R., Bunker, A. J., & McMahon, R. G. 2003, *MNRAS*, 342, 439
- Stanway, E. R., Bunker, A. J., McMahon, R. G., Ellis, R. S., Treu, T., & McCarthy, P. J. 2004a, *ApJ*, 607, 704
- Stanway, E. R., et al. 2004b, *ApJ*, 604, L13
- Steidel, C. C., Adelberger, K. L., Giavalisco, M., Dickinson, M., & Pettini, M. 1999, *ApJ*, 519, 1
- Steidel, C. C., Giavalisco, M., Pettini, M., Dickinson, M., & Adelberger, K. L. 1996, *ApJ*, 462, L17+
- Steidel, C. C., Hunt, M. P., Shapley, A. E., Adelberger, K. L., Pettini, M., Dickinson, M., & Giavalisco, M. 2002, *ApJ*, 576, 653
- Steidel, C. C., Pettini, M., & Hamilton, D. 1995, *AJ*, 110, 2519
- Stern, D., Bunker, A., Spinrad, H., & Dey, A. 2000, *ApJ*, 537, 73
- Stern, D. & Spinrad, H. 1999, *PASP*, 111, 1475
- Stern, D., Yost, S. A., Eckart, M. E., Harrison, F. A., Helfand, D. J., Djorgovski, S. G., Malhotra, S., & Rhoads, J. E. 2005, *ApJ*, 619, 12
- Taniguchi, Y., et al. 2005, *PASJ*, 57, 165
- Taniguchi, Y., Shioya, Y., Ajiki, M., Fujita, S. S., Nagao, T., & Murayama, T. 2003, *Journal of Korean Astronomical Society*, 36, 123
- van der Wel, A., Franx, M., van Dokkum, P., Rix, H.-W., Illingworth, G., & Rosati, P. 2005, *ApJ*, 631, 145
- Vanzella, E., et al. 2005, *A&A*, 434, 53
- Vanzella, E., et al. 2006, *A&A*, 454, 423
- Weymann, R. J., Stern, D., Bunker, A., Spinrad, H., Chaffee, F. H., Thompson, R. I., & Storrie-Lombardi, L. J. 1998, *ApJ*, 505, L95
- Yan, H., Dickinson, M., Giavalisco, M., Stern, D., Eisenhardt, P. R. M., & Ferguson, H. C. 2006, *ApJ*, 651, 24

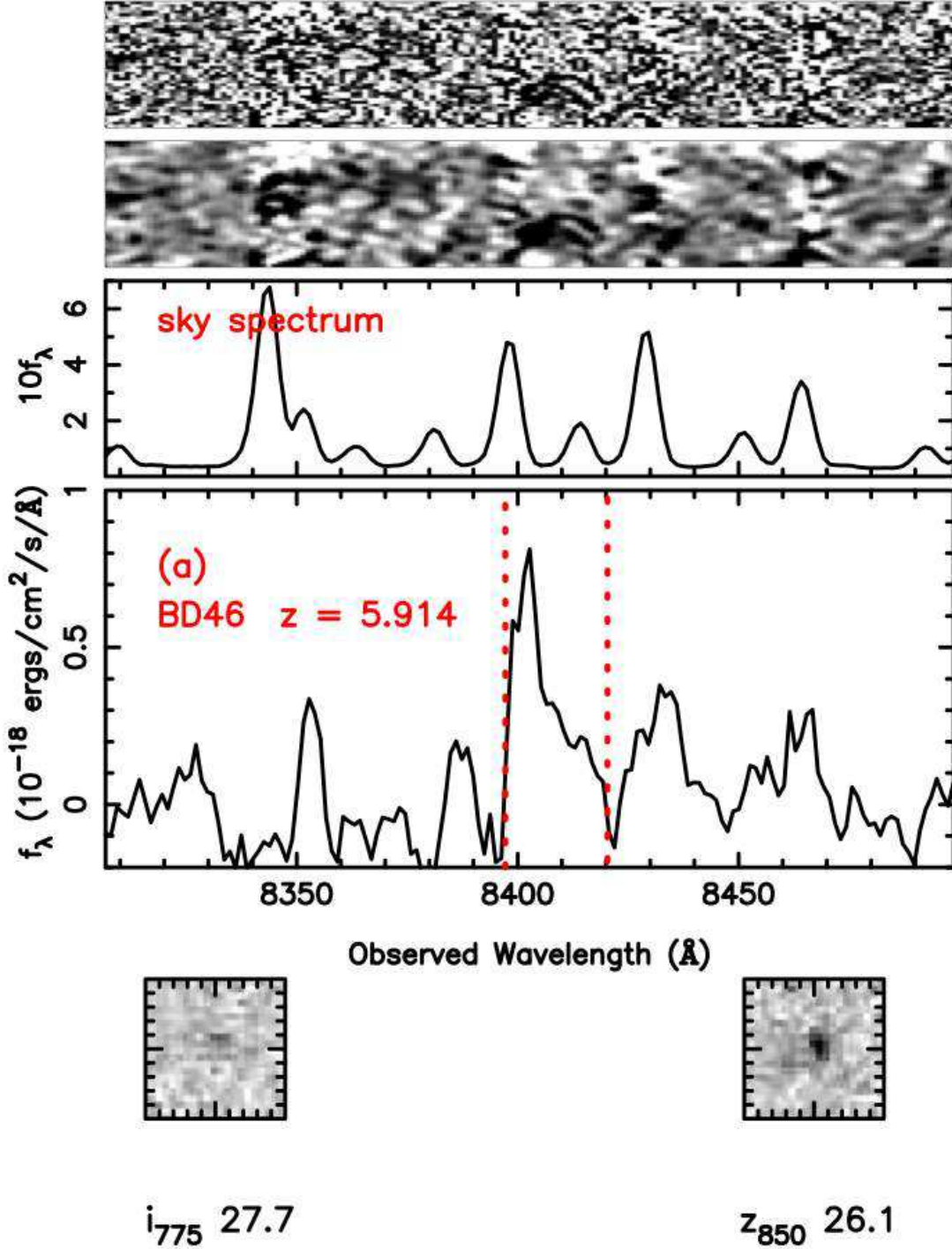
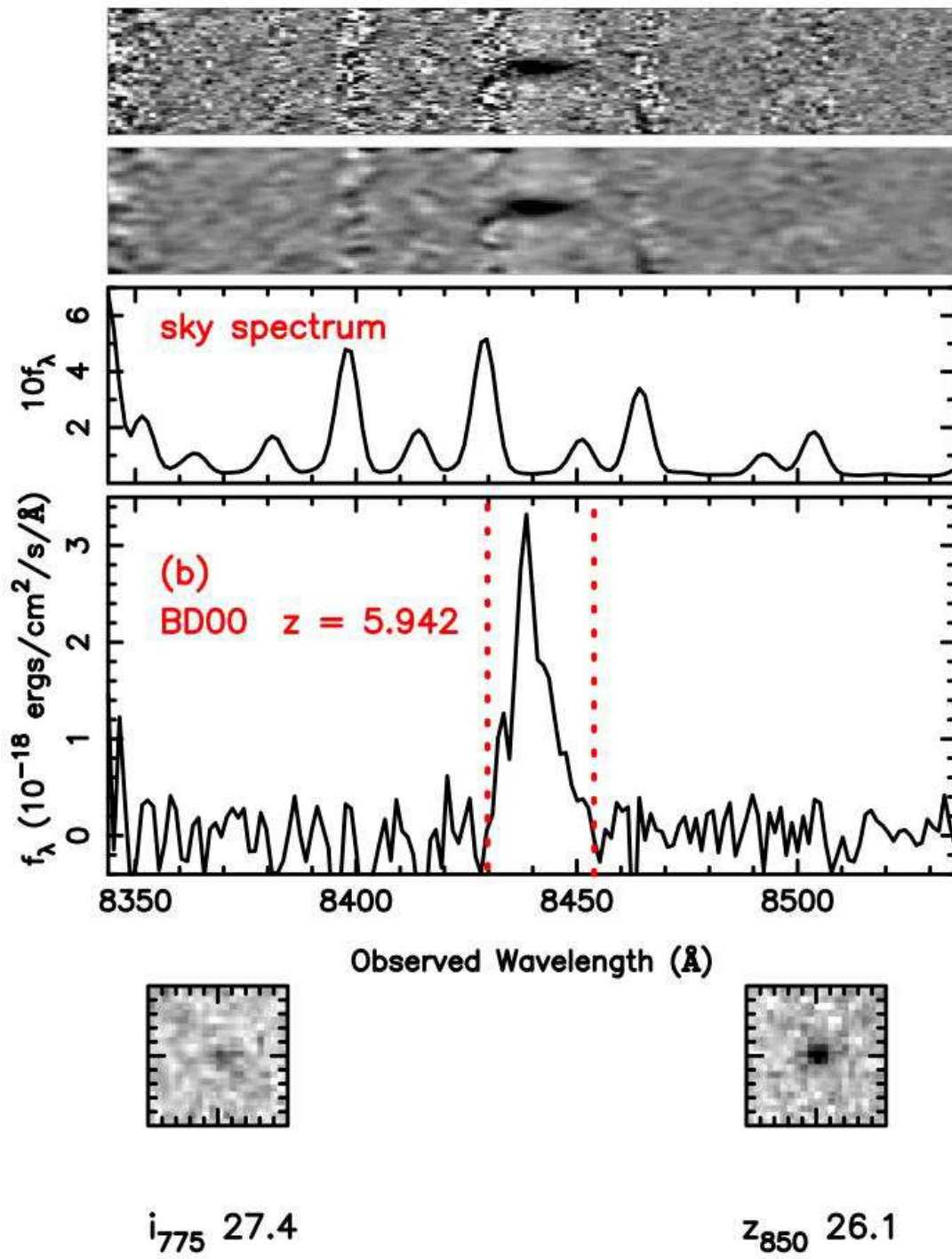
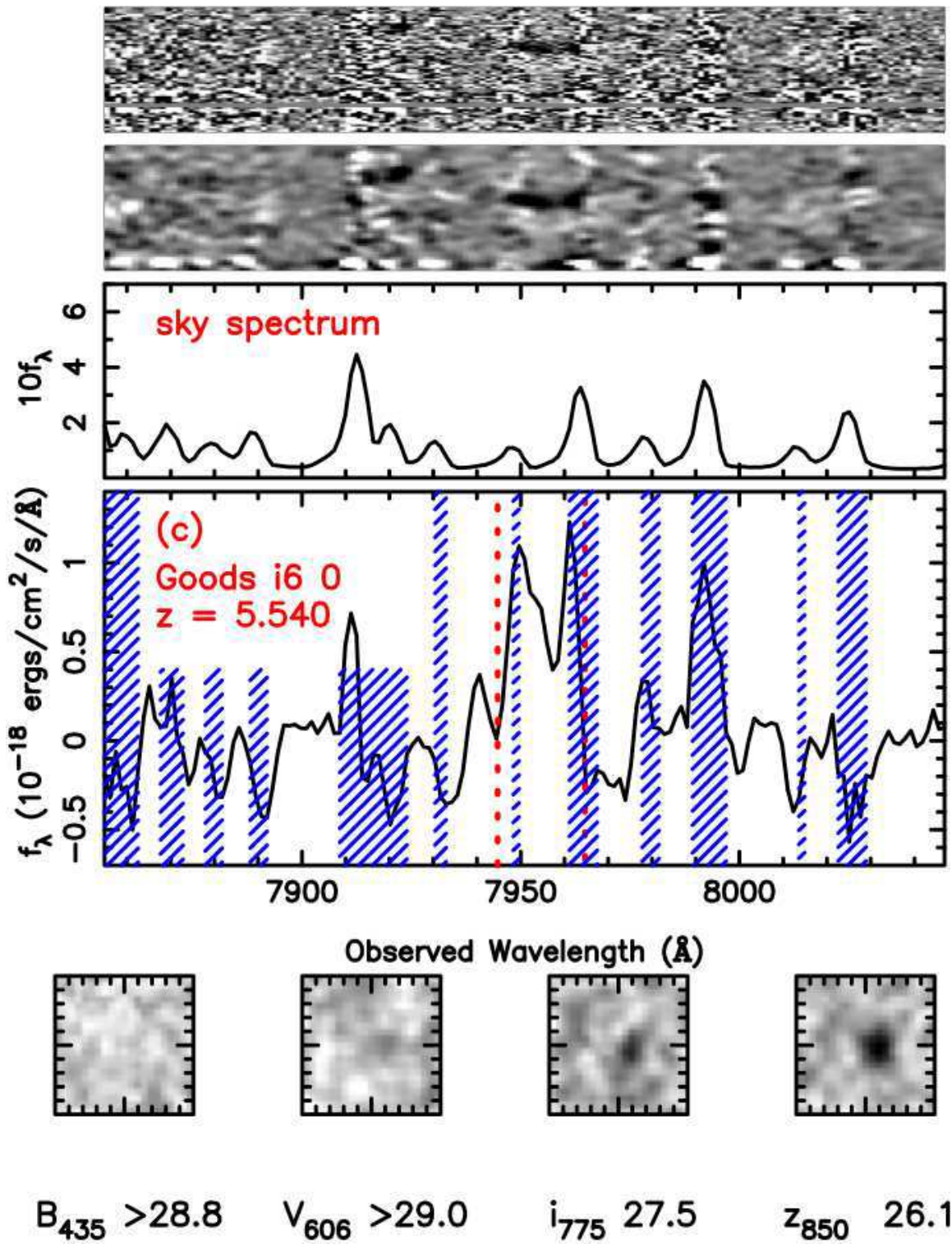
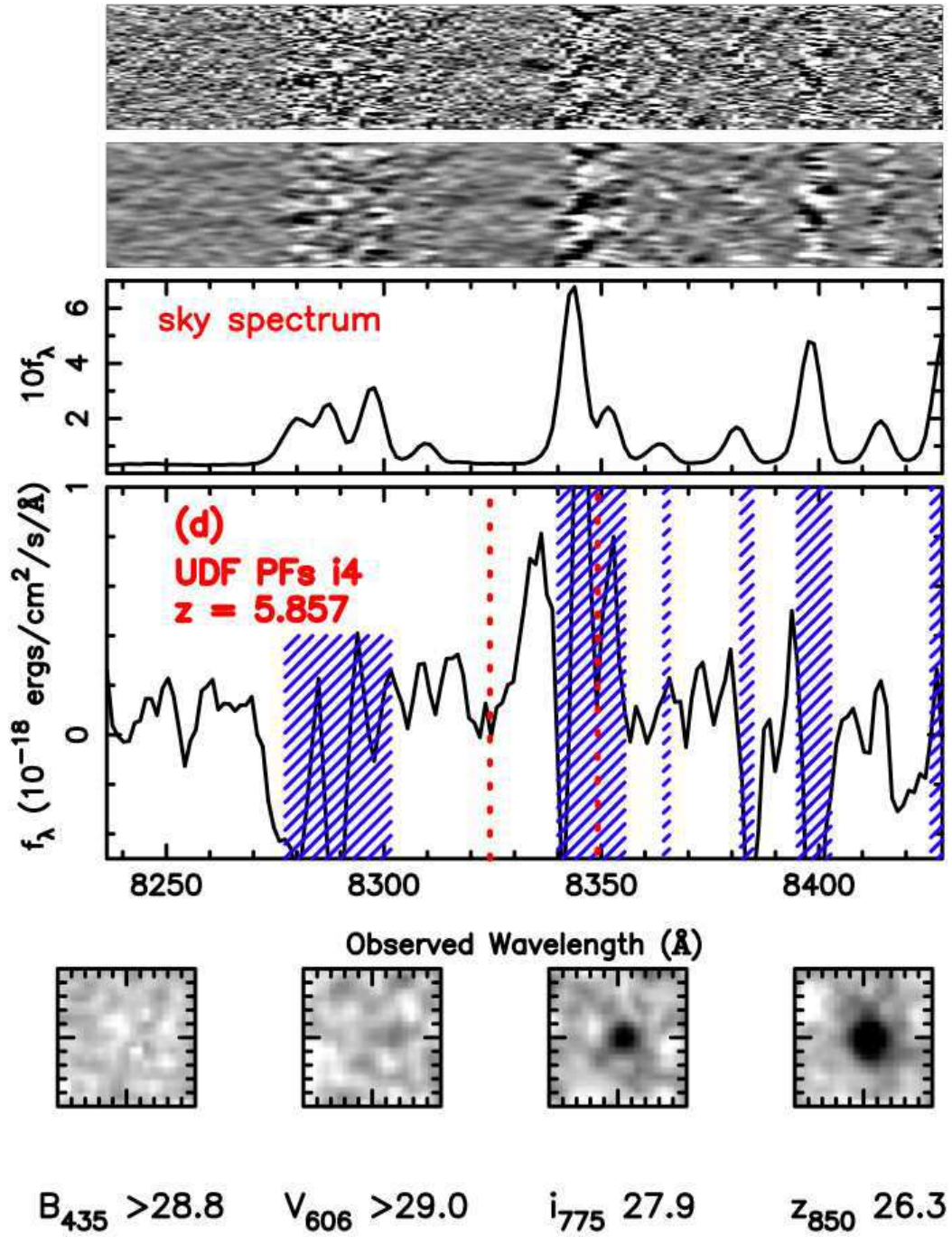
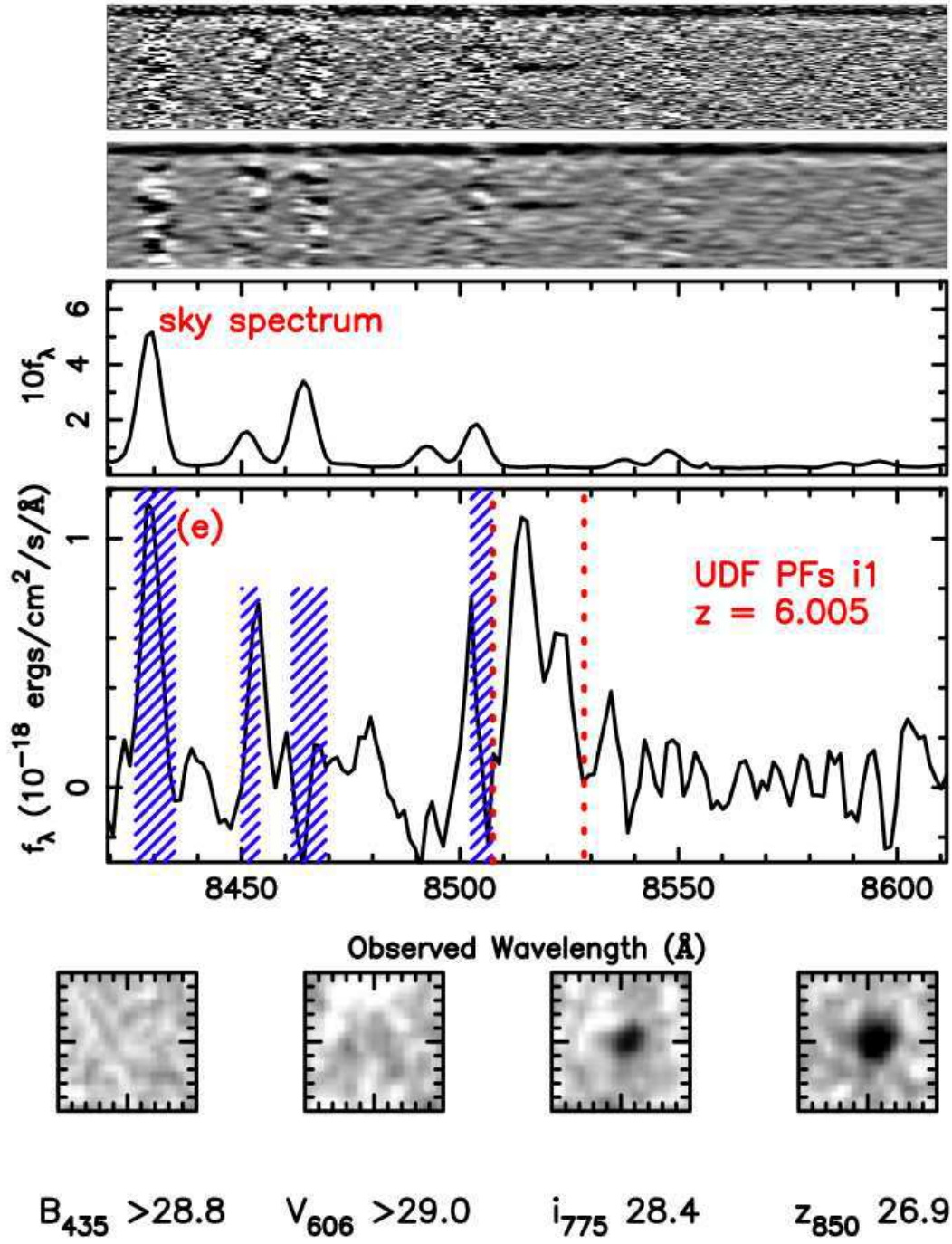


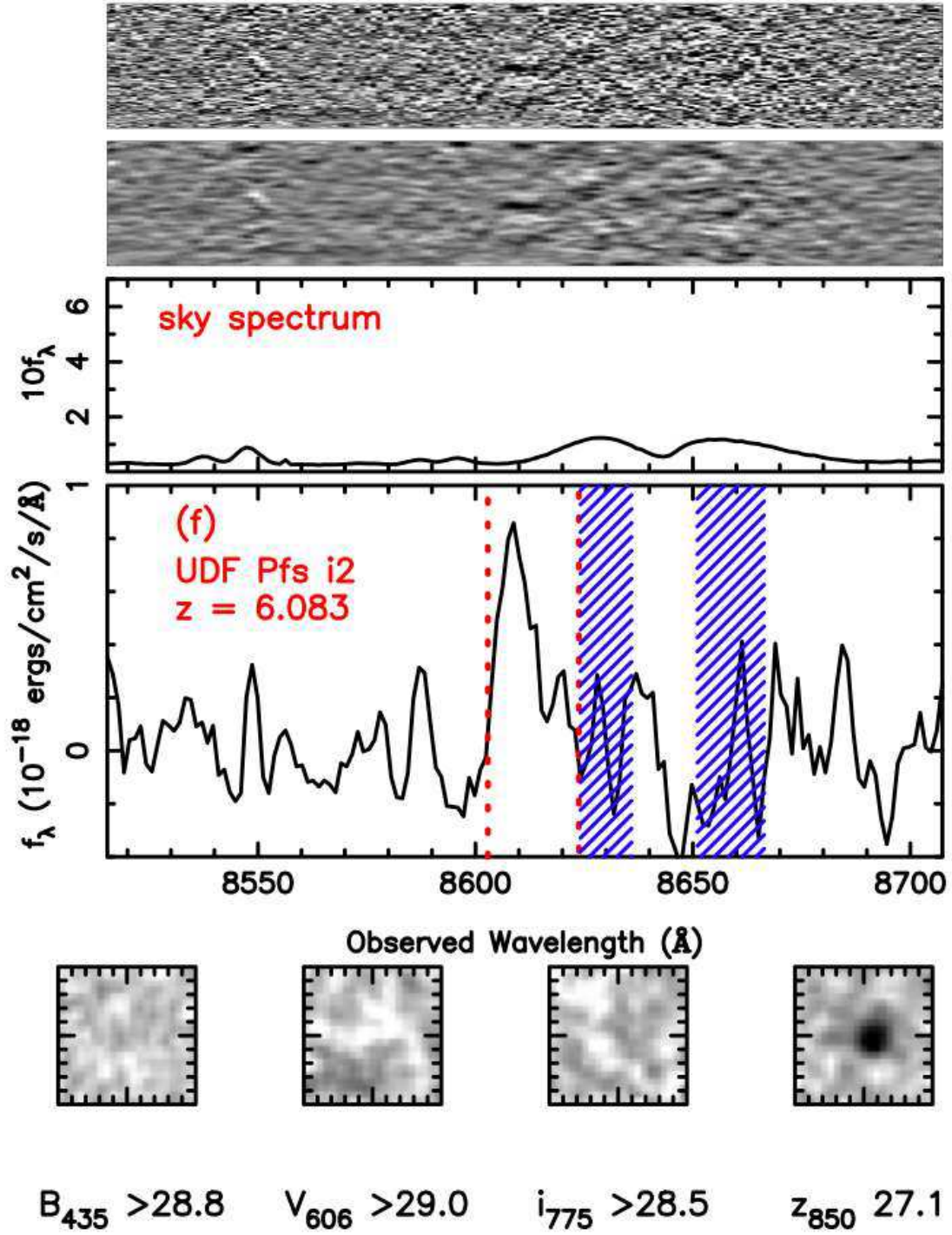
FIG. 2.— LRIS spectra and ACS imaging of emission line objects: two-dimensional unsmoothed spectra (upper panel), candidate Ly α emission (lower panel), and ACS imaging (lower postage stamps). Also shown is the two-dimensional $\sigma=1$ pixel Gaussian smoothed spectra of the sky (middle panel). Objects are (a) BD46, (b) BD00, (c) GOODS i6 0, (d) UDF PFs i4, (e) UDF PFs i1, and (f) UDF PFs i2. The postage stamps are $1''.0 \times 1''.0$. All upper limits given for the B_{453} , V_{606} , and i_{775} band fluxes are 2σ . The exposure times for the objects were 7200 s, except for the two CL1252 objects (BD46 and BD00) where the exposure times were 16200 s. Each one-dimensional spectrum has been smoothed with a 3 pixel boxcar filter, except BD00 and BD46. Vertical dotted lines delineate the region used for measuring line fluxes, equivalent widths, and FWHMs. For the UDF PFs objects, the blue cross hatched rectangles represent regions where strong skylines are present. The $i_{775} - z_{850}$ colors and the asymmetry of these line profiles are consistent with the emission lines from BD46, BD00, UDF PFs i1, and UDF PFs i2 being Ly α $\lambda 1215.67$. The other two emission lines (GOODS i6 0 and UDF PFs i4) are difficult to identify, due to skyline interference. We consider the implication that the features in these latter two sources are spurious and Ly α is undetected.











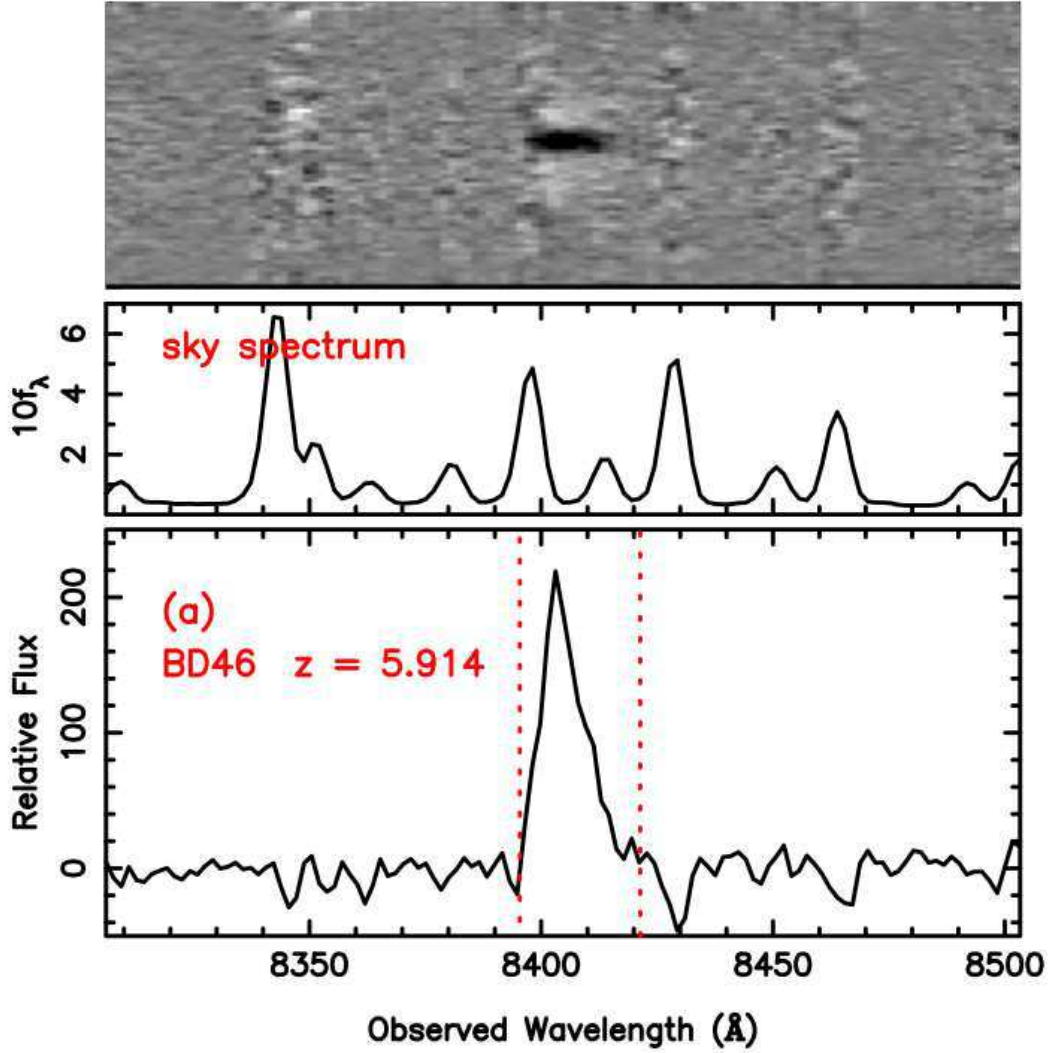
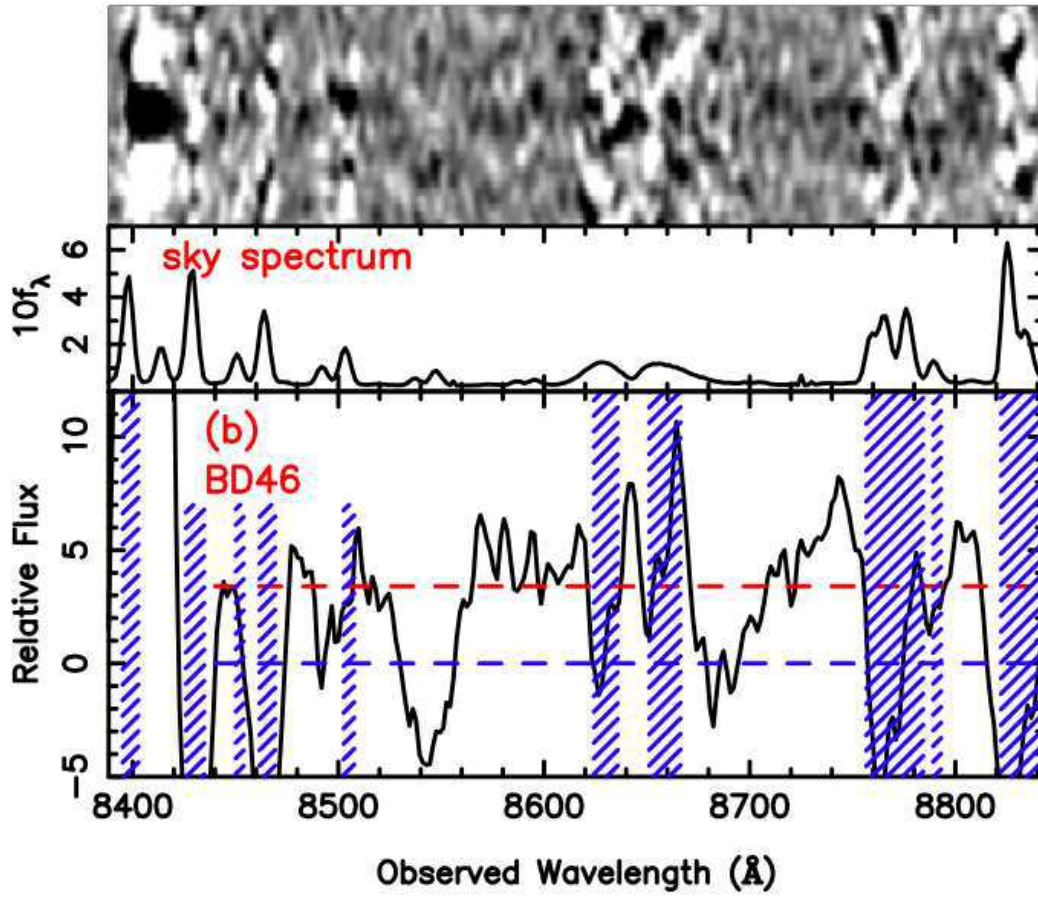


FIG. 3.— (a) FORS2 two- and one dimensional spectra of BD46 (LRIS spectrum shown in Fig. 2). The total exposure time is 22.3 hours. The Ly α emission occurs at 8406 \AA , consistent with the LRIS spectrum. (b) Shows the faint continuum of BD46 redward of the emission. The two dimensional spectrum has been smoothed with a $\sigma=1$ gaussian. The one dimensional spectrum has been smoothed with a 10-pixel boxcar filter. The red dashed line delineates the continuum of $f = 3.4 \pm 1.0$ counts \AA^{-1} .



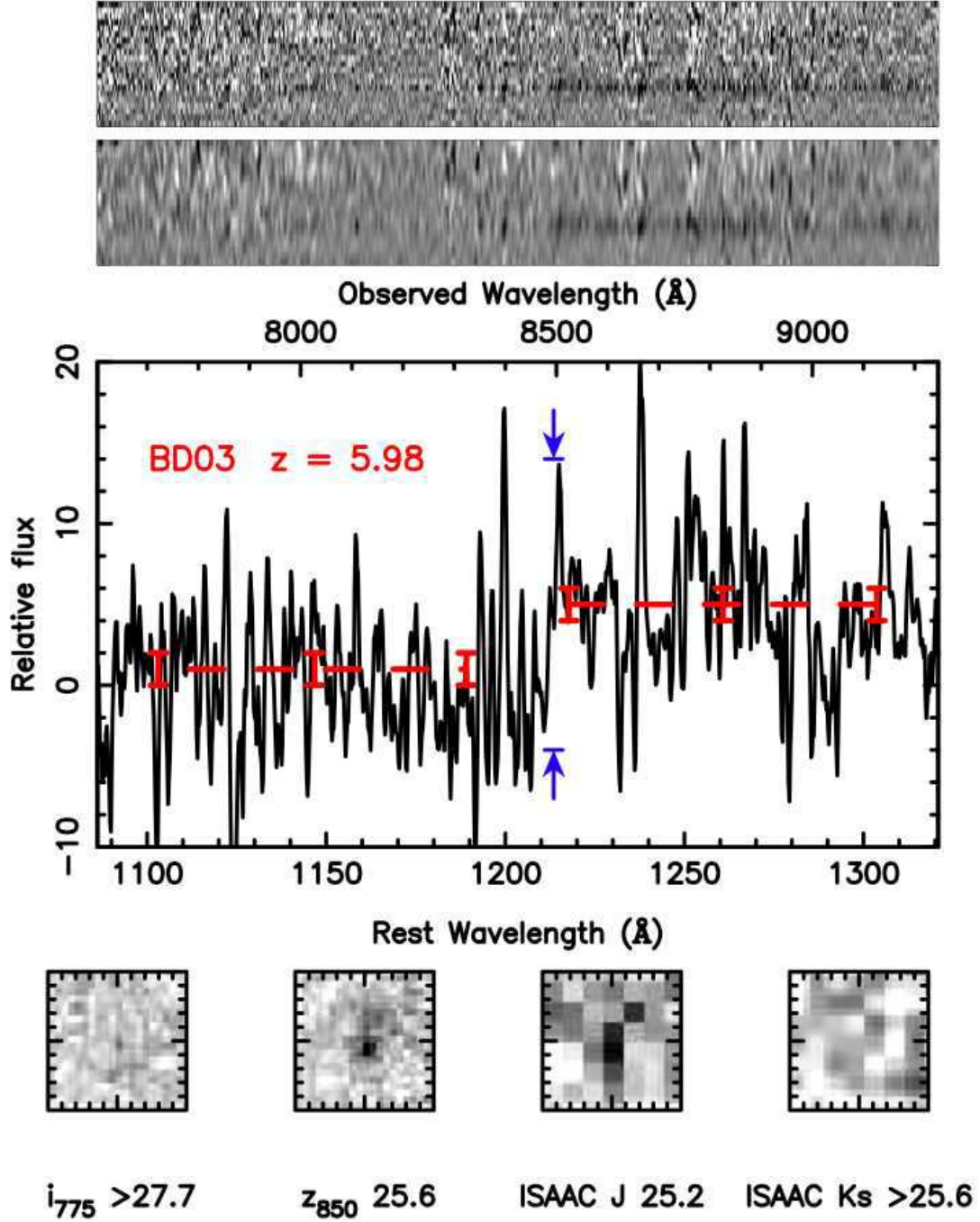


FIG. 4.— *FORS2* spectra and *ACS/ISAAC* imaging of *BD03* ($z = 5.98 \pm 0.1$). The upper two dimensional spectrum is unsmoothed, while the lower one is smoothed with a $\sigma=1$ pixel Gaussian. The extracted one-dimensional spectrum is smoothed with a 5 pixel boxcar filter. From left to right, the lower four images are i_{775} , z_{850} , J, and K. The total exposure time is 22.3 hours. The lower axis is the observed wavelength shifted to the systematic redshift $z = 5.98$. Blue arrows indicate the position of the continuum break. The dotted lines represent the wavelength region used to fit the continuum near the break, where error bars represent the 1σ error.

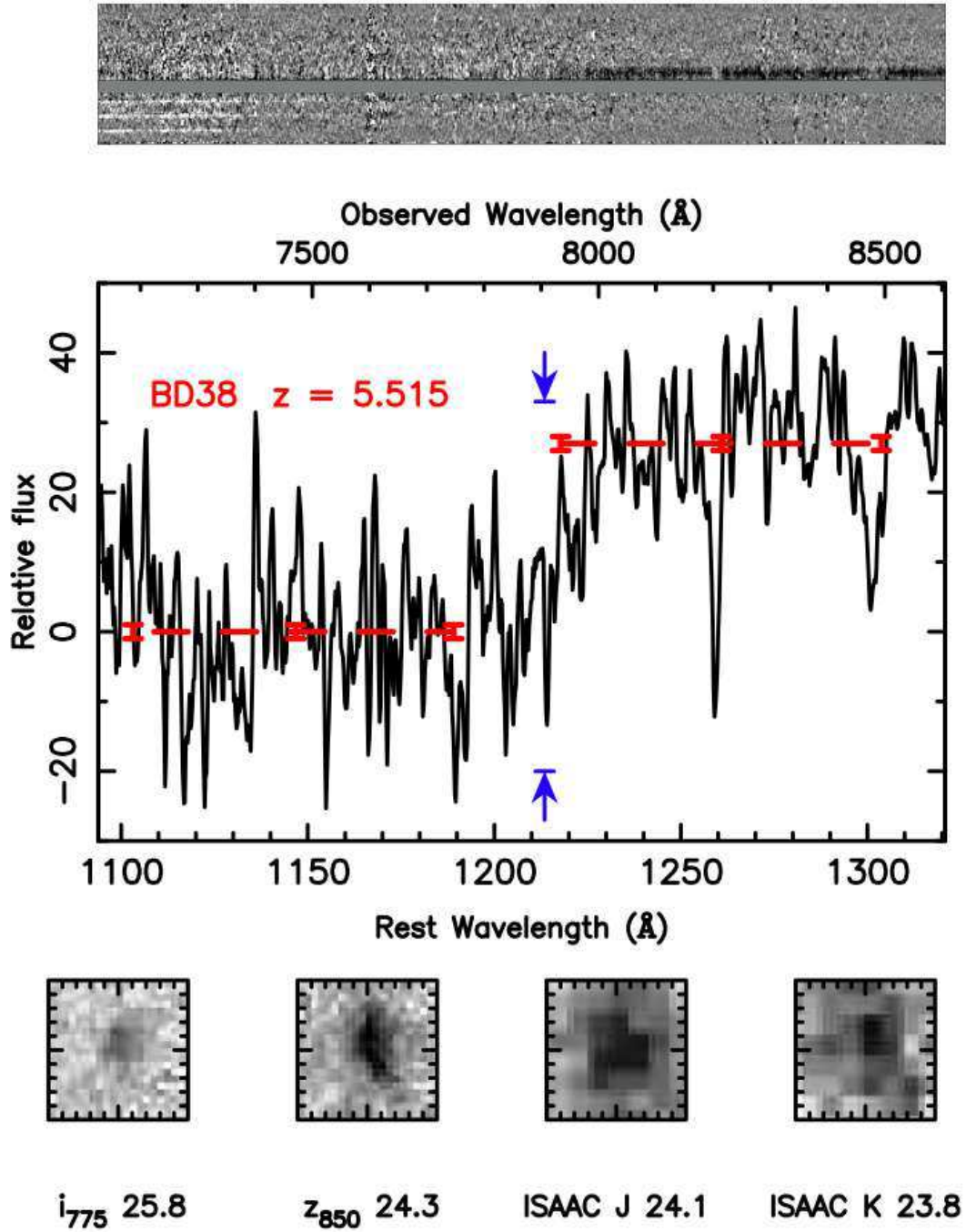


FIG. 5.— FORS2 spectra, ACS and ISAAC imaging of BD38: two-dimensional spectrum and extracted one-dimensional spectrum smoothed with a 5 pixel boxcar filter. From left to right, the lower four images are i_{775} , z_{850} , J, and K. The total exposure time is 22.3 hours. The lower axis is the observed wavelength shifted to the systematic redshift $z = 5.515$. Blue arrows indicate the position of the continuum break. The dotted lines represent the wavelength region used to fit the continuum near the break, where error bars represent 1σ error. A more complete spectrum is shown in Dow-Hygelund et al. (2005).